Analyst

Accepted Manuscript

This article can be cited before page numbers have been issued, to do this please use: E. Mauriz, P. Dey and L. M. Lechuga, *Analyst*, 2019, DOI: 10.1039/C9AN00701F.

ROYAL SOCIETY OF CHEMISTRY

rsc.li/analyst

Advances in Nanoplasmonic biosensors for clinical applications

Elba Mauriz[1*], Priyanka Dey[2] and Laura M. Lechuga[2]

[1] Department of Nursing and Physiotherapy, Universidad de León, Campus de Vegazana, s/n, 24071 León, Spain

[2] Nanobiosensors and Bioanalytical Applications Group, Catalan Institute of Nanoscience and Nanotechnology (ICN2), CSIC, BIST, and CIBER-BBN, Campus UAB, 08193 Barcelona, Spain.

Abstract Biomarkers are unquestionable biological indicators for diagnosis and therapeutic interventions providing appropriate classification of a wide range of health disorders and risk factors. Nonetheless, detection and quantification of biomarkers need to be tested with sufficient reliability by robust analytical methods in order to assure clinical performance in health care settings. Since the analytical performance is determined by the sensitivity and specificity of the method employed, techniques have been intensively refined in order to avoid misinterpretation of results and undesirable bias. Although biomarkers can be detected with the existing analytical techniques, to reproducibly quantify them in decentralized settings or remote locations with the required accuracy is still a challenge. Currently, only a few point-of-care devices for biomarkers evaluation are commercially available. Thus, more focused research efforts are needed to overcome those limitations in order to provide universal patient-centered care platforms.

To this end, plasmonic biosensors can be conveniently used as portable diagnostic devices for attaining timely and cost-effective clinical outcomes. The development of enhanced performances based on nanoplasmonics technology opens the way for sensor miniaturization, multiplexing and point of care testing. This review covers recent advances and applications of plasmonic and nanoplasmonic biosensors intended for biomarker diagnosis in the clinical practice, including cancer, cardiovascular and neurodegenerative diseases. The review specially focuses on: (i) recent progress in plasmonics developments including the design of singular nanostructured surfaces, (ii) novel chemical functionalization strategies for the appropriate incorporation of the bioreceptors and (iii) plasmonic applications as real operative devices in the clinical field. Future prospects in the use of nanoplasmonic sensor platforms for personalised quantification and management of biomarkers directly in body fluids will also be discussed.

1. Introduction

Biomarkers in body fluids are commonly utilized in clinical practice as diagnostic or prognostic indicators for the onset, progression and remittance of diseases.[1, 2] Biomarkers provide objective quantification of normal or pathological diagnostic outcomes and aid to predict the biological response after exposure to therapeutic drugs or environmental agents. The variety of biomarkers

View Article Online
DOI: 10.1039/C9AN00701F

that can be tested ranges from protein, gene expression profiles to blood and urine concentrations of drugs.[1, 3-6] In general, the classification of biomarkers relies on the sequence of events from exposure to disease onset, categorizing them as either diagnostic or monitoring markers. Diagnostic biomarkers allow the identification of a medical condition *via* genetic and pathophysiologic parameters while monitoring biomarkers assess the extent and progression of a disease by testing drug concentration or toxicity effects (FDA-NIH Biomarker Working Group).

Diagnostic or prognostic biomarkers allow for early detection of diseases and have been at the spotlight for researchers, especially for cancer biomarkers[2] as it promises significant improvement in chances of survival. Biomarker-based disease diagnostics relies on detecting the specific biomarkers associated to a disease and their presence in body fluids like blood, urine, saliva, sputum, cerebrospinal fluid (CSF), among others.[1, 3, 4] These biomarkers can exhibit a significant and specific concentration deviation (up/down regulation) in disease conditions compared to healthy conditions, followed by accurate and specific determination of concentration of the specific biomarker. This requires collection of body fluids, preferentially in a minimally invasive manner.

The phases of clinical diagnosis can be summarized as shown in Fig. 1. The usual laboratory procedures involve sample collection, sample pre-processing (for example, pre-concentration, DNA/RNA replication, growth incubation for pathogens, etc.), laboratory analytical test by expert technicians (to evaluate the biomarker concentration) and analysis of the data (comparison of the outcome to healthy condition). A summary of the complete procedure is then delivered to the medical team who decides the appropriate treatment. Though this analytical procedure provides reliable outcomes, an inherent limitation is its' inaccessibility at decentralized clinics, ambulatories, ambulances or hospitals itself, requiring in most cases an outsourced laboratory and, thereby, delaying critical care, particularly for cases like sepsis[7, 8] and other infections. Thus, medical diagnostics need a transformation towards portable diagnostic devices with quick turnaround time such that regular health biomarkers can be tested as point-of-care, at the doctor´s office, emergency rooms, ambulances, hospitals and even at home. This can be achieved by combining the sample pre-processing and the analytical test and read-out all into one simple-functioning, easy to-use, direct read-out point-of-care (POC) device platform. [9-11] This concept has been summarized in Fig. 1, where the research focus lies in POC device development.

View Article Online
DOI: 10.1039/C9AN00701F

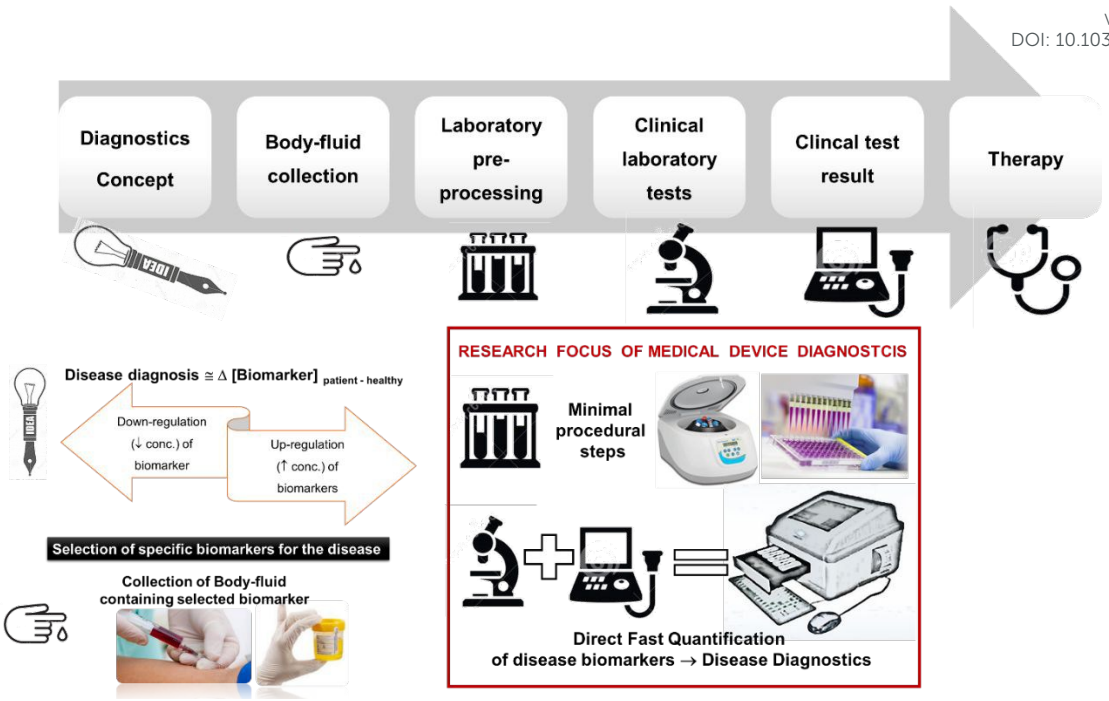

Fig. 1. Overview of the flow in clinical diagnostics in present and in the near future.

To accomplish this transformation, analytical methods can take advantage of biosensing-based platforms. Biosensors enable simultaneous and real-time detection of multiple biomarkers. They provide a measurable signal that can be quantitatively related to the amount of biomarker in the body fluids. An ideal biosensor for clinical diagnostics[12, 13] should fulfill the following characteristics: (a) be able to detect a specific biomarker in its clinically relevant range with a low limit of detection (LOD) and a minimum signal-to-noise (S/N) ratio >2 for high accuracy, (b) have a detection with high specificity (no cross-reactivity) and provide sensor-to-sensor reproducibility, (c) able to provide multiplexed analysis of several biomarkers related to the same disease, which would not only reduce the cost per test, but also will assure diagnostics accuracy, (d) minimal patient body-fluid (sample) required, (e) minimal operational complications and minimal additional reagents required, (f) fast testing turnaround times (potentially in minutes), (g) sensing instrument fairly compact and portable, as well as user-friendly and cost-effective, (h) sensor chips or substrates with a long shelf-life and stability in a wide working range of temperature and humidity.

An IDTechEx research report titled “Biosensors for Point-of-Care Testing: Technologies, Applications, Forecasts 2017-2027”, predicts biosensors for point-of-care testing market will grow to $33 billion by 2027, with molecular diagnostic devices as the main driver for this growth. The role of biosensors as clinical analytical tools has already been proven in the health care sector.

One of the most relevant examples that have popularized POC biosensor devices is the electrochemical based glucometers[14] that measure glucose levels from a drop of blood with digital read-out which is a must-have instrument for diabetic patients at home now-a-days. The other is pregnancy strips providing a visual color-based positive or negative read-out,based on gold nanoparticles changing colour due to aggregation upon interaction with pregnancy hormones. Products that are more recent utilize a smartphone as the read-out device, non-invasive wearable sensors[15], while others employ an injectable sensor material making the POC devices smarter and more lucrative.

Enzyme-linked immunosorbent assay (ELISA)[16] has been the gold standard in biomarker sensing with dominating market presence for laboratory-based technologies. Recently, with the drive towards POC devices, ELISA has been upgraded to lab-on-chip system by utilizing microfluidic technologies. Although ELISA has advantages of being a robust platform, it still requires long incubation and washing times along with the necessity of a detection label. Although plasmonic biosensing technology utilizes similar sensing principles as ELISA where the bioreceptor is immobilized onto a surface and the captured biomarker is detected, it is label-free and does not require extensive incubation/washing steps nor is labor-intensive. This in addition to the plausibility of plasmonic biosensor miniaturization, makes it an ideal technology for developing POC devices for clinical settings. Optical biosensors have thus gained immense limelight due to their capability of biomarker detection in real-time and significantly faster turnaround times with lower manual handling time. Recent reviews[3, 5, 12, 13, 17] justify the importance of optical nanobiosensors for biomarker detection.

A quick evaluation of the scientific community´s effort in the field of nanoplasmonic biosensors is portrayed in Fig. 2, which shows the publication contribution, in the past decade, of advances in nanoplasmonics covering all aspects of nanoplasmonic sensor substrate and/or associated optical technologies including Surface Plasmon Resonance (SPR), Localized Surface Plasmon Resonance (LSPR) and Surface enhanced Raman scattering (SERS). In order to gain a better understanding of specific technologies that have moved towards clinical biomarker detection, we analyze the above publications in two categories: “general” (all and any advances) and “biomarker sensing” (publications which demonstrate some clinically relevant studies). Fig. 2 (right-most bar for % translation) clearly depicts that SPR and LSPR technologies have moved into clinical applications for biomarker detection while overall nanoplasmonic and SERS domains are predominantly in the research phase.

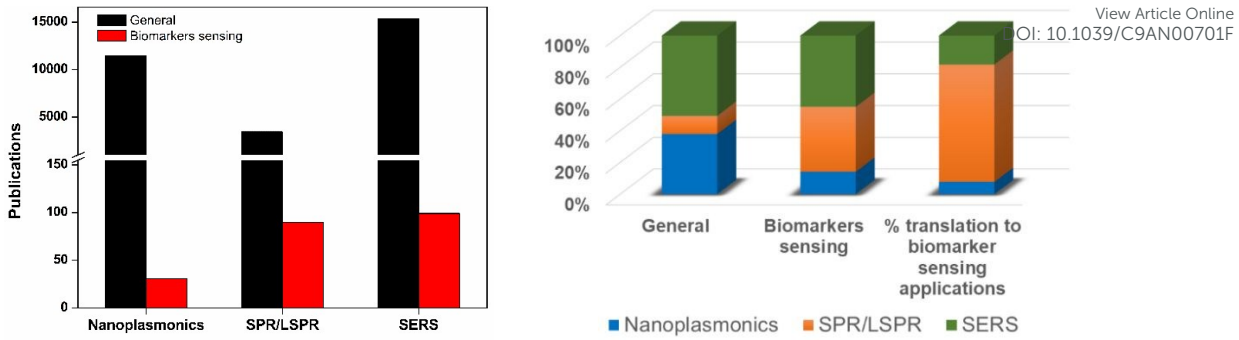

Fig. 2. Statistics of published papers in the last decade (2007-onwards) demonstrating the higher translation of SPR/LSPR technologies employed for biomarker sensing applications. Here, "nanoplasmonics" refers to the work done in the overall area of plasmonic sensors and their applications in various optical technologies. *Source: Web of Science*.

This review contains a critical discussion of the recent advances in clinical biomarker evaluation employing nanoplasmonic biosensors. Special attention has been focused on SPR and LSPR biosensor devices employed as diagnostic, predictive, prognostic or monitoring tools for assessing cancer, cardiovascular, autoimmune and neurodegenerative diseases. Current progress in the analytical performance of biomarker evaluation in biological media has also been discussed. Finally, we consider different approaches in multiplexing and miniaturization of plasmonic biosensors as steps towards designing fully-automated POC instruments.

2. SPR and LSPR biosensors: working principles

SPR. Both SPR and LSPR are examples of surface plasmon (SP) based sensors. When an incident light interacts with a noble metal, photons induce a collective oscillation of the free electrons in the conduction band of the metal generating surface plasmon polaritons (SPP), a form of electromagnetic (EM) waves, propagating at the sensor metal-dielectric interface. It is important to note that only a p-polarized electromagnetic or transverse magnetic wave is able to sustain SPPs. The simplest geometry sustaining SPPs is that of a flat interface between a metal and a dielectric medium with dielectric constants of opposite signs. Gold, silver, copper, and aluminium are some of the metals that feature a negative real and a small positive imaginary dielectric constant and hence are able to support SPPs. In terms of choice of the sensor, silver (Ag) has the largest negative real dielectric constant and hence is more sensitive to refractive index (RI) changes, but has poor chemical stability as it is readily oxidized in air. On the other hand, gold (Au) has lower RI sensitivity than Ag but has higher stability, as well as higher chemical affinity which can be employed to easily functionalize the sensor surface for target biomolecule capture. Thus, Au has a higher employability in plasmonic biosensors and SPR sensor chips are often

made of a thin gold film of approximately 50 nm coated onto a dielectric substrate like glass or silica.

The bulk RI sensitivity defined as the ability of the plasmonic sensor to detect changes in the RI is widely used to understand the effect of different parameters on the sensor performance. The bulk RI sensitivity (S_B) is defined as (1)

$$S_B = \frac{d\lambda_r}{dn_B} \quad \text{..... (1)}$$

where λ_r is the SP excitation wavelength (resonant wavelength) and n is the RI of the medium in contact with the sensor surface. The review by Špačková and co-workers[18] discuss in detail the effects of various parameters on S_B including the type of supporting EM mode (decay length), resonant wavelength, excitation geometry, and properties of the sensor. Among them, one of the main factors that affect S_B is the localization of the EM mode. The generated electromagnetic plasmonic waves extend to around 100–400 nm (SPR decay length) from the metal-dielectric interface making it capable of detecting any biomolecular binding event *via* dielectric RI change occurring within that range in the dielectric medium.

Additionally, the ability of a plasmonic sensor to measure minute changes in the RI is directly proportional to S_B and, furthermore, inversely proportional to the width ω of the resonant spectral feature being monitored. The figure of merit (FOM) (equation 2) is a combination of these parameters and serves as a quantitative comparison of sensing efficiency among different nanostructures. The importance and comparisons of FOM has been discussed in dedicated reviews.[13, 18]

$$FOM_B = \frac{S_B}{\omega} \quad \text{..... (2)}$$

A combination of the above factors and the ability to tune the optical response specifically and sensitively culminates into a limit of detection (LOD) with a sensitivity of 10^{-6}–10^{-7} Refractive Index Units (RIU), making SPR a desirable choice for optical biosensor technology. Fig. 3(a) and (b) shows a standard SPR biosensor configuration along with data read-out of change in reflection angle (θ) as a snap shot measurement, as well as a real-time measurement.

On the other hand, several optical device configurations have been explored depending on the in coupling of the light to excite the resonance, SPR devices can employed either a prism, grating waveguide or fiber optic to achieve the excitation of surface plasmons.[19, 20] The incident light coupling in fibre optic sensors are guided by total internal reflection inside the fibre core waveguide. At the fibre core waveguide-metal interface a evanescent field is generated. This configuration is increasingly becoming popular due to numerous advantages such as smart size,

high resolution, flexibility, and miniaturization, which allow sensing in harsh conditions and over long distances. A recent review by Tokel and co-workers[6] discusses the role of the prism dielectric constant, energy-momentum conservation and the plasmon resonance angle which is highly sensitive to minute changes in the refractive index (RI) at the metal-dielectric interface. A SPR biosensor setup in the frequently used prism-coupled Kretschmann configuration is shown in Fig. 3(a). The main advantage of such a configuration is that it allows monitoring of the incidence angle continuously and hence real-time detection is possible.

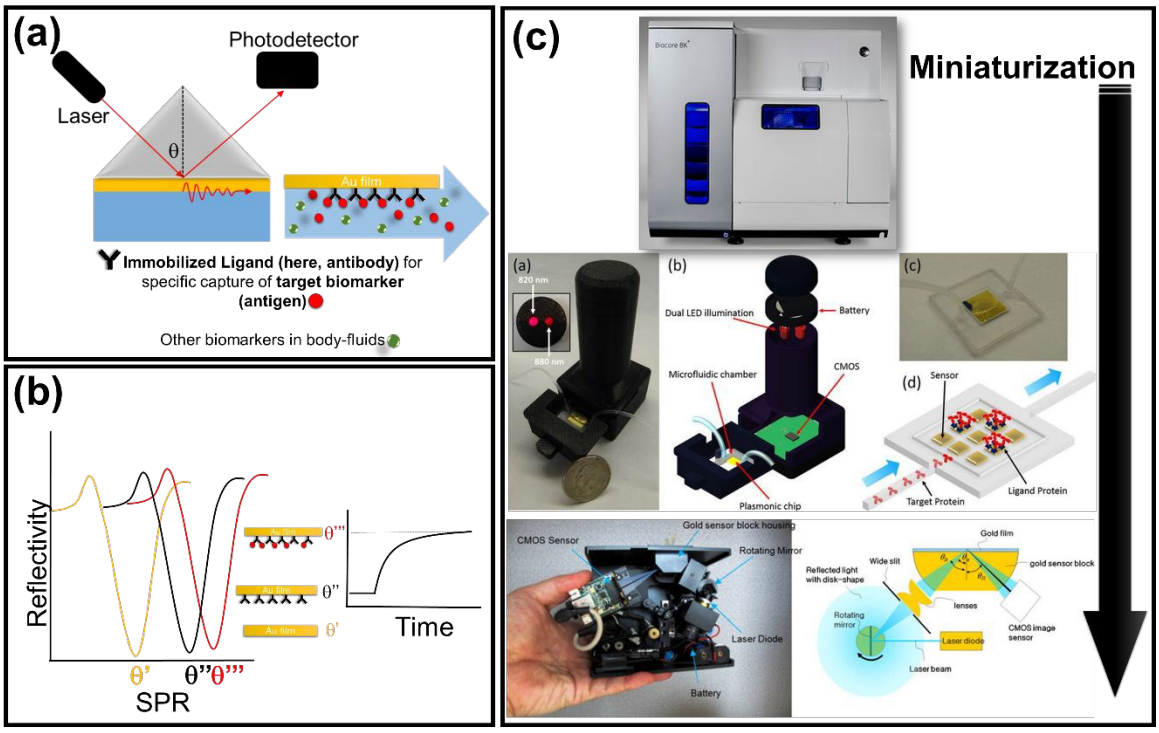

Fig. 3. Schematic overview of (a) the biosensing detection (read-outs) for SPR on a thin gold film and (b) SPR read-out change in refection angle θ. (c) Miniaturization of the SPR instrument: from large commercial SPR (Biacore, GE Healthcare) (left), to hand-held devices[21] (middle) and plan-held[22] (right) Adapted with permission from *Scientific reports*, 2014, 4, 6789 and *Sensors and Actuators B: Chemical*, 2010, **150**, 1-6. Copyright (2010) Elsevier.

Furthermore, the light coupling strategies need to be efficient and for commercial high-throughput devices can cost a fair share. Miniaturization of SPR devices (as shown in Fig. 3c) into portable bench-top[21] and palm-top[22] set-ups has thus been investigated for boosting usability in clinical settings. Microfluidics, as well as smart optical components have revolutionized this transformation.[4, 17, 19, 23-27] Interesting reviews of lab-on-chip integrated sensor devices justify the strategies and advantages of such approaches for miniaturization.[28] Researchers have also included LED light source as opposed to laser, CMOS (Complementary Metal Oxide

Semiconductor) detector instead of CCD (Charge Coupled Device) camera, as well as a battery power source in order to minimize the size and the cost of the SPR instrument, making it attractive for POC market.[8, 21, 22] Some of the above features, which have mainly been implemented in the research phase, have been depicted in Fig. 3c. Commercial SPR devices which are still comparatively bulky, are available from approximately 20 companies and costs approximately 50-300k euros. Thus, the size and cost are major hurdles for its market penetration to every decentralized clinic in the world. The other major drawback of SPR instruments is its limited multiplexing capability; they often require multiple sensors chips (similar to Fig. 3c-middle panel-d) in addition to multi-flow channels requiring complex microfluidics. Various reports and reviews suggest improved nanoscale manufacturing, microarray assay development and microfluidics channel design as some of the choices for achieving miniaturization and improving cost-effectiveness.[4, 19, 29-32] A review by Masson provides an outlook of SPR biosensors, its limitations and benefits.[33]

SPRi. Following the initial discovery of SPR microscopy in 1998 where SPP field was used to image microscopic interfacial structures, researchers explored the use of surface plasmon resonance imaging (SPRi) for biosensing applications. SPRi allows detection and imaging in the entire sensor area and provides an added benefit of multiplexed detection, as opposed to SPR. SPRi sensors have been based on intensity, angular wavelength, phase, and polarization interrogations. A more extended explanation of SPRi fundamentals can be found in reviews by Wong and Olivio.[34] One review compares SPR and SPR imaging[35], while others discuss the importance of sensor interface design, biofunctionalization[36, 37] and multiplexing in SPRi[25]. Though SPRi is a high throughput multiplexed technique, it suffers from reduced detection sensitivity of about one order of magnitude compared with SPR sensing. This reduction is due to the adaptation of a less compact optical configuration with a less sensitive mode of intensity-based measurement and less sensitive detectors. The review by Liu and coworkers[38] summarizes the recent developments in SPRi sensitivity discussing signal enhancement and/or amplification, and noise suppression. A more recent and detailed review[39] of SPRi encompasses the significance of optical platforms, functional coatings, biomolecular interactions (drug–receptor, protein–protein, protein–DNA, protein–cell) and their applications of a broad variety of analytes (nucleic acids, proteins, bacteria). Though there has been some progress in the field of SPRi, it is not yet the most suitable technique for clinical applications.

LSPR. When metallic nanostructures interact with light, localized field oscillations are observed inspiring the name "localized" SPR i.e., LSPR. In this situation, part of the incident light is

View Article Online
DOI: 10.1039/C9AN00701F

absorbed and part is scattered. Both absorption and scattering are greatly enhanced when the LSPR resonance mode is excited. The large amplification observed in extinction (absorption and scattering) can be explained by an analytical solution of Maxwell´s equation with spherical boundary conditions, referred to as Mie theory which illustrates the extinction spectra of a nanoparticle. To extend this theory to more complex nanoparticles shapes and calculate dielectric constants at different wavelengths, the Modified Long Wavelength Approximation (MLWA) of Mie theory is used as stated below.[40]

$$C_{ext} = \frac{24\,\pi^2 R^2 \varepsilon_m^{\frac{3}{2}} N}{\lambda \ln(10)} \frac{\varepsilon_i}{(\varepsilon_r + \chi\,\varepsilon_m)^2 + \varepsilon_i^2} \quad \ldots\ldots\ldots\ldots\ldots\ldots\ldots\ldots (3)$$

where R is the radius of the particle, λ is the wavelength of the incident light, ε_m is the dielectric constant of the surrounding medium, $\varepsilon = \varepsilon_r + i\varepsilon_i$ is the complex dielectric constant of the bulk metal, N is the electron density, and χ accounts for the shape of the particle (equals to 2 for a sphere and up to 20 for high-aspect ratio particles like nanorods). This proves the importance of the plasmonic nanoparticle physical properties in LSPR sensing, as opposed to that in SPR. It is also worth mentioning that with the increase in nanoparticle (NP) size, the relative contribution of scattering to extinction increases, with scattering observed for NPs ≥30 nm. The above equation (3) defines the importance of the different parameters including the shape of the NP, wavelength of incident light, type of material, and last but most importantly, the surrounding media and its dielectric constant. For a given nanoplasmonic system, a change in C_{ext} and λ_{max} (which lies in the visible region for Au and Ag, making them highly important) will be observed if the media surrounding of the nanoplasmonic system changes i.e., changes in its dielectric constant (ε) and refractive index (n) related by $\varepsilon = n^2$. This has been utilized in determining analytes or biomarkers that can bind to a functionalized nanoplasmonic surface, where the refractive index change translates into a LSPR λ_{max} shift. Thus, the LSPR Δλ read-out plot would be similar to that of SPR θ plot shown in Fig. 3b. Furthermore, the shift in LSPR frequency upon biomolecular binding is described by the following relation: [40]

$$\Delta\lambda = m(\Delta n)\left[1 - \exp\left(\frac{-2d}{l_d}\right)\right] \quad \ldots\ldots\ldots\ldots\ldots\ldots\ldots\ldots (4)$$

Where, m is the refractive index sensitivity, Δn is the change in refractive index induced by the biomolecule, d is the effective biomolecular layer thickness and l_d is the electromagnetic field decay length (approximated as an exponential decay length).

Therefore, the continuous thin gold film used for SPR would not be sufficient for LSPR. LSPR sensor substrates demands nanostructured features onto a substrate, this is an added complexity and cost factor as opposed to SPR technologies. The electromagnetic field decay length for metal

nano-surfaces is of the order of 10–40 nm for NPs from the sensor surface as compared to 100–400 nm for SPR continuous metal films. This thus improves surface sensitivity of the nanoplasmonic substrates for biomolecular sensing which happens closer to the sensor surface. As compared to SPR, LSPR has negligible contribution from the bulk sensitivity and bulk temperature fluctuations and thus feature high nano-surface sensitivity. SPR requires an external light coupling method, whereas, light is directly coupled to the sensor for LSPR. This thereby reduces the complexity of the instrumentation and with the market availability of portable sensitive spectrometers, LSPR demonstrates strong potential for clinical diagnostic applications. A more complete description of SPR, LSPR and their comparison can be found in our previous reviews[41] and other literature reports[42].

3. Nanoplasmonic biosensors

Research in engineering and optimization of plasmonic nanostructures supporting SPP has been immensely boosted due to its application as LSPR biosensors.[43-46] The simplest form of substrate fabrication methodology is the bottom-up approach where colloidal plasmonic nanoparticles (NPs) are firstly synthesized and further employed for biosensing applications. In this domain, extensive effort has been directed towards plasmonic NP synthesis (shape, size, composition variants), linker directed self-assembly (morphology variants) for improving the stability, optical response and reproducibility of such colloidal nanostructures.[44, 47-50] Although, simple and cheap to synthesize and covers a wide range of LSPR resonant wavelength of 400-1000 nm, its low shelf-life restricts the applicability of colloidal NPs in clinical applications, especially where laboratory-like controlled storage facilities are not available. Other factors include batch-to-batch variation in production, presence of stabilizing agents that interfere with biosensing, as well as the large handling or shipping volume (in colloidal form) limiting transportability.

In contrast, top-down nanostructures formed *via* lithography[51-58] benefit from the long shelf-life, easy transportability and ease of usage as sensor chips for detection. This has instigated a research interest in fabrication techniques to obtain reproducible high performance nanoplasmonics. Various fabrication techniques have been employed including e-beam lithography, mask lithography, etc.[57, 58] An interesting bottom-up lithographic technique referred to as the colloidal lithography has gained limelight as it offers an easy control and fabrication of various shapes and sizes onto the sensor substrate while still being a low-cost technology.[51, 56] Nanoimprint lithography is another low-cost and easy to implement technology which is gaining momentum

for nanoplasmonic structure fabrication.[57] Furthermore, nanostructures featuring increase of polarizability *via* multipolar resonance, plasmon coupling for boosting LSPR, as well as employing optical antenna structures (like arrays of nanocrescents, nanostars, nanocross etc. with varying pitch) utilizing the lightening rod effect has been employed, few of which has been shown in Fig. 4.

For example, plasmonic nanodiscs have been widely investigated where studies have focused on fabricating them with control over the height, nanogap, diameter, as well as employing a trunk for elevated nanodiscs.[55, 59, 60] Another novel methodology uses Blu-ray discs as the base substrate which inherently offers nano-gratings and which require only a one-step coating with nanoplasmonic metals as Au or Ag (Fig. 4).[61] Other structures like nano split rings, nanocrescents, nanopillars have also gained interest. Nanoholes, have both LSPR properties, as well as extraordinary transmission (EOT) properties.[8] Interesting research is being conducted in forming various array types with the nanoholes and features that resemble nanocups.[62] In summary, taking into account the increase in sensitivity, the plasmonic nanostructures can be categorized into colloidal NPs with lowest sensitivity, followed by nanoholes and nanodiscs and, finally, by other varied structures as nanopillars, nanocrescents, nanorings etc., offering highest sensitivity. Nanoholes and nanodisc plasmonic structures operate in the wavelength range of 450-1000 nm and are typically fabricated using colloidal or nanoimprint lithography.[8] They offer higher shelf-life and better scalability and hence are favored for mass production than other nanostructures like nanopillars etc. which otherwise feature higher sensitivity. Nanopillars, nanocrescents[55] require complicated fabrication technologies that are difficult to scale up and are less amenable for biofunctionalization. Until now, nanodiscs and nanoholes have been dominating the field.

View Article Online
DOI: 10.1039/C9AN00701F

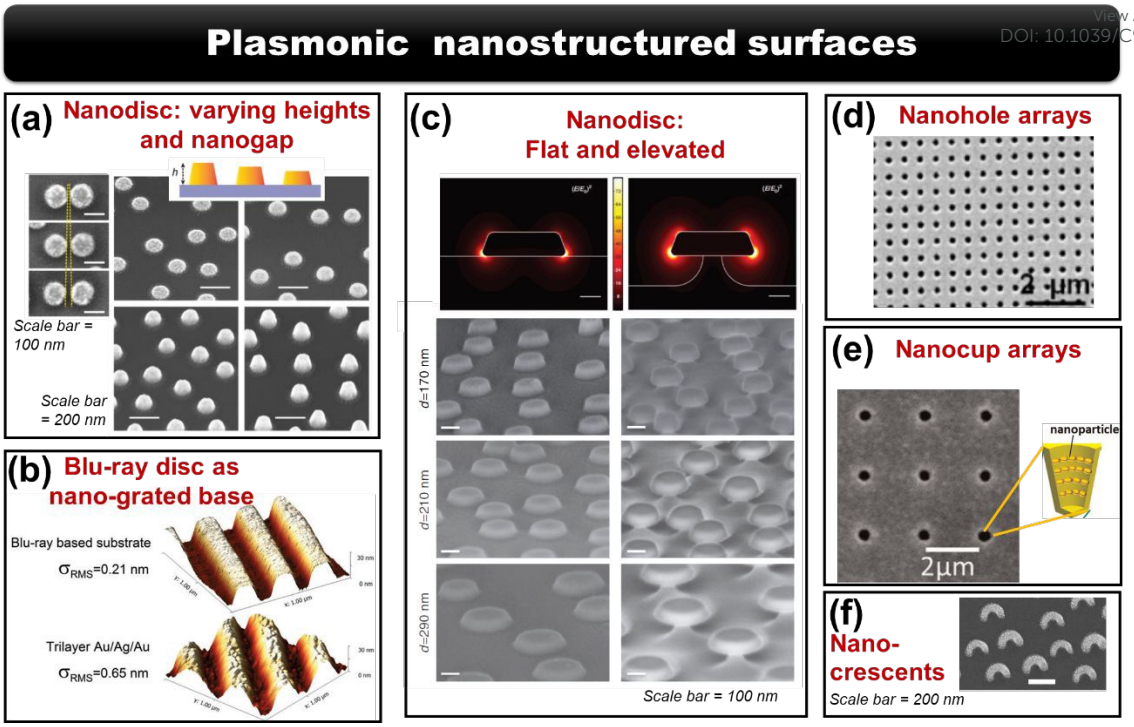

Fig. 4 (a) Nanodiscs with varying height and nanogaps[55], (b) Blu-ray disk coated with nanoplasmonic metals[61], (c) nanodiscs both flat on the surface and elevated[59], (d) nanohole arrays[8], (e) nanocup arrays[62] and (f) nanocrescents[55]. Adapted with permission from *Advanced materials,* 2016, 28, 4658-4664 and *Journal of biophotonics*, 2018, 11 (Copyright Wiley); *Light, science & applications*, 2017, 6; and *Biosensors & bioelectronics*, 2015, 67, 237-242). Copyright (2015) Elsevier.

4. Nanoplasmonic biosensors for clinical biomarkers analysis

4.1. Neurodegenerative diseases

The prognostic use of plasmonic biosensors for the diagnostics of neurodegenerative diseases demands the characterization of aggregation prone proteins related to the etiology of Alzheimer's, Parkinson and Prion diseases. Although there is an increasing interest in the development of neurodegenerative diagnostic tools, particularly for Alzheimer's disease (AD), plasmonic biosensors are still under-utilized in this domain. This gap is especially pronounced for the diagnosis of Parkinson disease biomarkers, wherein the scarce use of optical biosensors mainly relies on quantum dots-related approaches.

Amyloid beta peptides and tau proteins are the most frequent biomarkers employed as diagnostic targets for Alzheimer disease. Among them, amyloid beta levels have been detected and evaluated in serum and cerebrospinal fluid (CSF) by SPR, LSPR and SPRi biosensors. The most common amyloid beta oligomers detected are 1-40 and 1-42, since they are frequently overexpressed in

amyloid plaques as a result of the degradation of amyloid precursor protein (APP). For instance, a shape-code LSPR nanoplasmonic biosensor for multiplex detection of amyloid beta (A beta) 1-40, A beta 1-42 and tau protein at 34.9 fM, 26 fM and 23.6 fM levels, respectively, was developed in mimicked blood by functionalizing heterobifunctional polyethylene glycol coated gold nanoparticles with specific antibodies and detecting directly the target proteins.[63] The shape-code plasmonic biosensor was based on the optical properties of gold nanoparticles of three different shapes and sizes that allow the detection of distinct conjugated biomolecules from separate colored spots and plasmonic spectra. Determination of Alzheimer protein biomarkers onto the antibody functionalized gold nanoparticles was measured by quantifying Rayleigh light scattering shifts after analyte binding through dark-field microscope, a spectrograph, and a CCD camera.

When using SPR biosensors, A beta 1-42 have been detected in the 22 to 440 pM range with waveguide-coupled bimetallic chips.[64] The plasmonic biosensor makes use of Ag/Au films (Au as an outer layer) in order to improve the sensitivity by increasing the reflectance change obtained in an intensity interrogation detection mode. The assay proved to detect selectively A beta 1-42 from A beta 1-4a oligomer although results in human biofluids such as blood or cerebrospinal fluid were not shown.

Other prominent biomarker of Alzheimer's and Parkinson disease, detected either in plasma or CSF samples, is tau Protein which is associated with defective aggregation of microtubules and abnormal expression in neurodegenerative diseases.

Recently, Truong *et al.* described an immunoassay capable of detecting tau and phosphorylated tau proteins, characteristic of tau pathologies, at pM in human sera of AD patients employing a SPR fiber sensor.[65] The detection method consisted of the conventional Tau antibody immobilization onto a thiol Self-Assembled Monolayer (SAM) followed by direct detection of total and phosphorylated tau proteins. The analytical performance was tested using real blood samples of 40 participants over 65 years, divided equally into experimental and control groups. The results obtained contribute to define the rule of unphosphorylated tau proteins in the progress of AD disease since concentrations of phosphorylated tau proteins (3-fold higher) were less increased than tau proteins (6-fold higher) in AD disease patients when compared with the control group. This suggests that unphosphorylated tau proteins are more likely to be produced in blood of AD patients than phosphorylated tau proteins. In addition, the compact format of the SPR device envisages its potential application for POC testing of tau proteins present in human blood in the POCT mode.

Another SPR approach has demonstrated the determination of human tau 381 protein at 10 fM levels in undiluted plasma[66] by a multichannel platform. The detection format consisted of a DNA aptamer/antibody sandwich assay over a tailored mixed monolayer on the sensor surface. Results were validated by ELISA showing a 1000-fold sensitivity improvement for SPR, allowing Tau determination in both spiked and native samples (see Fig. 5).

View Article Online
DOI: 10.1039/C9AN00701F

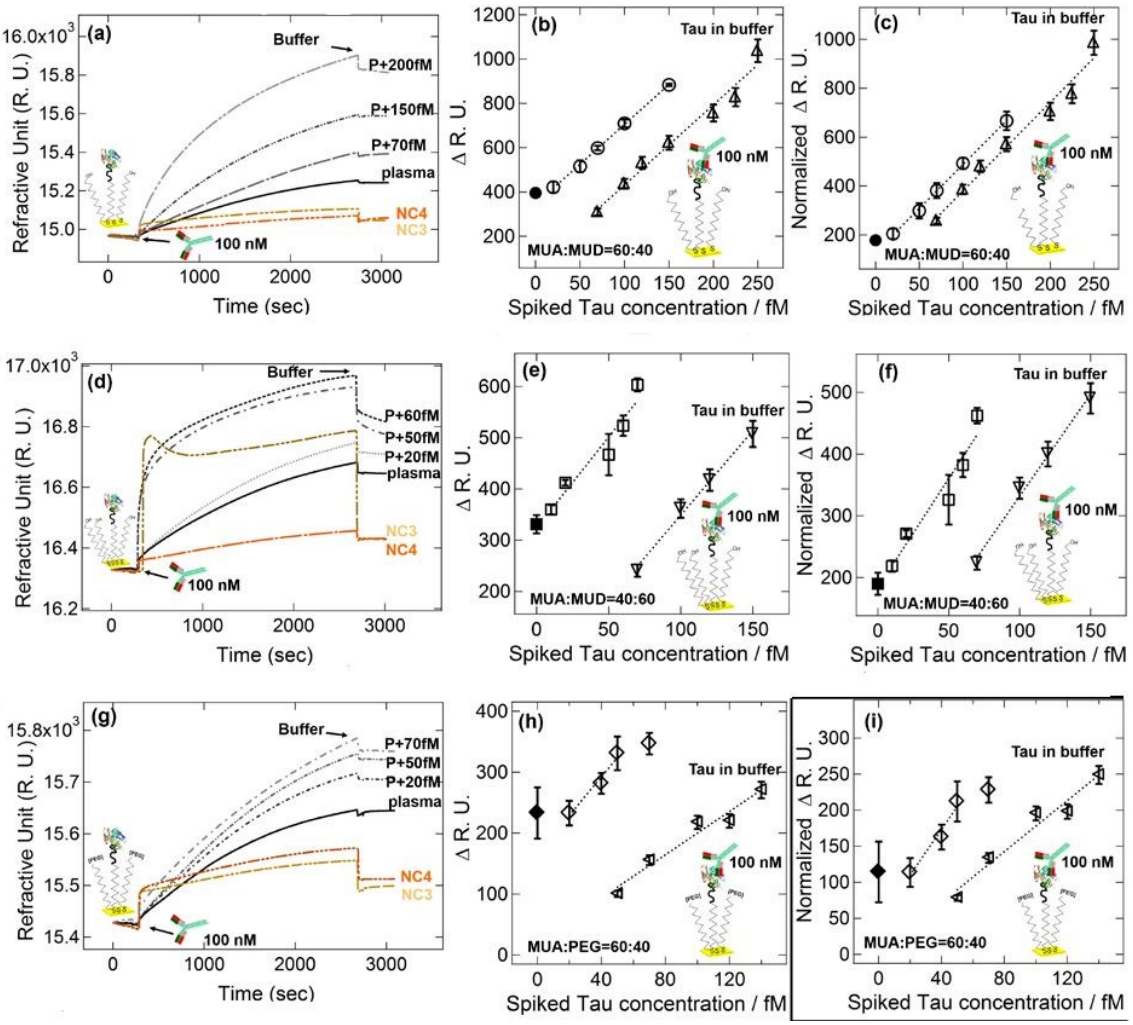

Fig 5. SPR Analysis in plasma for three different chip monolayer compositions: 60% 11-mercaptoundecanoic acid (MUA):40% 11-mercaptoundecanol (MUD), 40% MUA:60% MUD, 60% MUA:40% PEG monolayers. (a), (d), (g) Real-time SPR evaluation of anti-Tau adsorption following exposure to different Tau concentrations spiked directly into plasma, P. (b), (e), (h) Δ R.U plots obtained by calculating difference in R.U. signals in buffer before and after plasma exposure. (c), (f), (i) is where the Δ R.U signal has been normalized with respect to the average Δ R.U. signal of all non-specific controls (NC). The filled data point marker in the Δ R.U and normalized Δ R.U. plots represents the plasma signal with no spiking. Representative NC3(anti-recombinant human complement) and NC4 (aptamer control sequence) plots are also shown in (a), (d) and (g).

Finally, an original approach involving SPR detection by employing multiwalled carbon nanotubes (MWCNTs) was reported by Lisi *et al*.[67] The functionalization of the nanotubes with a secondary Tau antibody afforded tau determination using a sandwich detection format over a previously immobilized primary antibody layer. A signal amplification of 102-fold was obtained in comparison with the direct and conventional unconjugated format, reaching a detection limit of 125 pM. The major limitation of the study is referred to the lack of analysis in real biological fluid since all the measurements were performed in buffer or in artificial cerebrospinal fluid. Nevertheless, further improvement in avoiding matrix interference would permit its potential transfer as a disposable device for POC testing.

Additionally, prion protein detection has been explored by SPR as a promising method for screening of other neurodegenerative diseases such as the Creutzfeldt Jakob syndrome and its variant Bovine spongiform encephalopathy (BSE).[68] Lou *et al.* described an aptamer-based assay that exploits the magnetic properties of microspheres to selectively capture prion proteins from complex environments, while preventing interference effects of other compounds present in the same sample. The assay comprised of the fabrication of magnetic nanoparticles and the subsequent immobilization of aptamers by glutaraldehyde cross-linking. At this stage, Prion proteins could be captured by the functionalized magnetic nanoparticles, although the amphiphilic copolymer was required to embed and isolate prion proteins from the environment. Finally, the generation of an alternating magnetic field was needed to release the labeled prion proteins and allow SPR detection. In spite of the number of multiple steps and the complicated assay sequence, prion proteins were evaluated in the 0.01-1000 ng mL^{-1} range and demonstrated good correlation with determination in serum samples.

The identification of amyloid fibrils as final products of α-synuclein aggregation pathways may be associated with the diagnosis and treatment of several neurodegenerative diseases. A nanoplasmonic biosensor was employed to investigate the formation of amyloid fibrils as a result of the aggregation of α-Synuclein proteins by using the chiroptical properties of helical fibril proteins to induce chiral nanoparticle assembly of gold nanorods.[69] Furthermore, the detection of infectious prion proteins is reported by monitoring the circular dichroism (CD) signal at the longitudinal plasmon wavelength after the arrangement of prion fibrils to gold nanorods as a consequence of the helical assembly of gold nanoparticles to the fibrilar surface. The formation of helical nanorods was associated with the identification of α-Synuclein protein fibrils in samples of human brain homogenates of patients with Parkinson's disease in contrast with the absence of optical activity observed in human healthy brain samples. The plasmonic technique therefore opens a route not only to the early detection of the Parkinson disease and novel therapeutic

strategies but also to a methodology that provides better understanding of the characterization of aggregated species and template-driven plasmon chirality.

4.2. Cancer biomarkers

The detection of cancer biomarkers as predictive, diagnostic and prognosis tools by plasmonic biosensors takes advantage of their multiplexing performance for the rapid and simultaneous screening of a variety of biomarkers. The selection of the most appropriate cancer biomarkers is crucial since a wide range of biomolecules could be included in this category according to the clinical findings. Thereby, a universal classification relying on the biological nature of the biomarker should be considered in order to include the main cancer biomarkers categories, namely: proteins, exosomes, nucleic acids and circulating tumor cells.

4.2.1. Proteins

The interest in the determination of protein cancer biomarkers relies on their relevance to demonstrate translational alterations in genetic related oncology disorders while permitting the quantification of deviations in body fluid concentrations between cancer patients and healthy subjects. Among proteins, the most significant and commonly reported biomarkers for cancer screening have been PSA, VEGF and CEA.

PSA

"The prostate-specific antigen (PSA) has been extensively used as the most accepted biomarker for the diagnosis of prostate cancer, in spite of its low accuracy and limited specificity.". PSA is a glycoprotein produced by the prostate gland commonly measured in serum as the sum of free (fPSA) and complexed PSA. Although total PSA (tPSA) concentrations above 10.0 ng mL^{-1} may indicate high probability of prostate cancer and tPSA concentrations below 4.0 ng mL^{-1} are normally found in healthy subjects, patients with tPSA levels between 4.0 ng mL^{-1} and 10.0 ng mL^{-1} are included in a diagnosis grey zone. Therefore, the assessment of novel biomarkers in serum is essential for the diagnosis of prostate cancer malignancy. Since sensitive determinations of fPSA are difficult to obtain by conventional methods, as concentration in serum is below 1 ng mL^{-1}, the fPSA/tPSA ratio has recently become a relevant diagnosis value for differentiating between benign and malignant states. In this sense, several SPR and combined nanoplasmonic approaches have reported PSA detection of either total or free/total serum fractions, involving from immunoassay to microcontact patterning and aptamer-based assay deposition techniques.

Ertuk *et al.* described a bottom-up functionalization strategy based on the fabrication of SPR sensor chips with PSA imprints.[70] The method makes use of methacrylate derivatives and UV polymerization to imprint the PSA protein *via* microcontact patterning. The design of the SPR

biosensor chip allowed PSA determination at highly sensitive levels (91 pg mL^{-1}), improving the limit of detection of conventional analytical methods by an order of magnitude. Clinical analysis was performed in spiked human serum samples (1/4 diluted) of prostate cancer patients. Additionally, relevant analytical parameters such as specificity against another proteins (HSA and lysozyme) and association kinetic analysis were also reported, while good results were observed for recovery, reusability and correlation with ELISA immunoassays. This method shows an alternative patterning strategy to conventional molecular imprinting techniques enabling a high specificity and binding capacity of the template molecule, while maintaining long-term conformational stability of the recognition layer. These features are inherent advantages that enable its application as a POC detection platform.

Another approach involving a micropatterned plasmonic strategy is described by Breault.[71] The method employs a dual detection system that combines the wavelength interrogation of a four-channel SPR instrument and a fluorescence microscope mounted on the same SPR platform. SPR biosensor chips were fabricated by photolithography to generate microhole arrays thus permitting fluorescence detection from the solution side of the micropatterned gold film and SPR interrogation using the interface between the glass prism and the gold film. The fabrication of a micropatterned surface by incorporating microhole arrays allowed the improvement of SPR response in 2-3 orders of magnitude. Likewise, the use of a sandwich-immunoassay format comprising a capture anti-PSA antibody immobilized at the sensor chip and a labeled horseperoxidase detection antibody incubated with Ampliflu™ Red solution increases the sensitivity when using fluorescence detection in comparison with the SPR format. The singular combination of SPR and fluorescence assays in a single chip using the same microfluidics provided highly sensitive PSA determinations at clinical concentrations between 142 pg mL^{-1} and 1.42 μg mL^{-1}.

Discrimination between PSA free and total serum fractions from benign and malignant disease state has been reported by Jiang and co-workers using a dual-channel SPR immunosensor[72]. Total PSA fraction was measured directly with a linear range from 1.0 to 20.0 ng mL^{-1}, whereas the free fraction was detected *via* an asynchronous competitive inhibition immunoassay enhanced by gold nanoparticles, reaching a linear range between 0.010 to 0.40 ng mL^{-1}. By measuring simultaneously total and free PSA serum fractions in each channel the f/t-PSA ratio was calculated showing significant differences between benign prostatic hyperplasia and prostatic cancer patients. The application of this methodology provides meaningful clinical information about prostate cancer diagnosis in addition to the analytical results.

Single detection of PSA free fraction has also been reported using a LSPR-coupled fiber-optic biosensor.[73] A direct immunoassay was employed, based on the anti-PSA antibody immobilization onto a SAM modified sensor chip. The major contribution is the fabrication of a gold nanodisc at the fiber end facet allowing the reusability of the dielectric-metallic hybrid

interface and a detection limit of 0.85 ng mL^{-1}. The development of a a miniaturized multiplexed POC device is suggested although. clinical applications were not demonstrated since PSA evaluation was only done in buffer.

Another LSPR system with functionalized gold nanodiscs array is presented by Khan *et al.*[74], where PSA detection was performed by using DNA aptamers as specific receptors. The technique takes advantage of the symmetry of gold nanodiscs thus providing detectable responses in a short range near the vicinity of the sensor surface. Another strategy presented was the functionalization of gold nanostructures with PSA specific aptamers providing a limit of detection of 1.49 ng mL^{-1} within a linear range of 1.7 to 20.4 ng mL^{-1} in buffer. The interference in human serum was also tested showing good recovery values. Likewise, the reusability of the gold sensor was also demonstrated by removing the applied aptamers with $NaBH_4$ solution.

VEGF

Vascular endothelial growth factor (VEGF) is a hypoxia-inducible protein that promotes vasculogenesis and angiogenesis. VEGF appears frequently upregulated in most human tumors and it is a valuable cancer-specific protein biomarker for assessing the disease status during cancer progression and metastasis. SPR biosensing of VEGF is primarily based on aptamer or antibody assay formats.

One of the most singular approaches involve the application of rolling circle amplification (RCA) to enhance the SPR signal by targeting different VEGF domains with two DNA aptamers, employed as capture and detection probes, respectively. VEap121 is named as Aptamer 1 and provides high affinity to the receptor binding domain of $VEGF_{165}$ while VEa5 or Aptamer 2, shows high binding affinity to the $VEGF_{165}$ heparin binding domains. The aptasensor is based on the immobilization of Aptamer 1 for monitoring VEGF in real-time. The RCA process makes use of hybridization with the primers of the aptamer 2- polystyrene microspheres complex[75] to increase the VEGF sensitivity. A limit of detection of 100 pg mL^{-1} with a linear range from $1x10^{-12}$ to $1x10^{-5}$ g mL^{-1} was achieved. The method shows the potential applicability of RCA to assist SPR signal enhancement although lacks results with real samples (see Fig. 6).

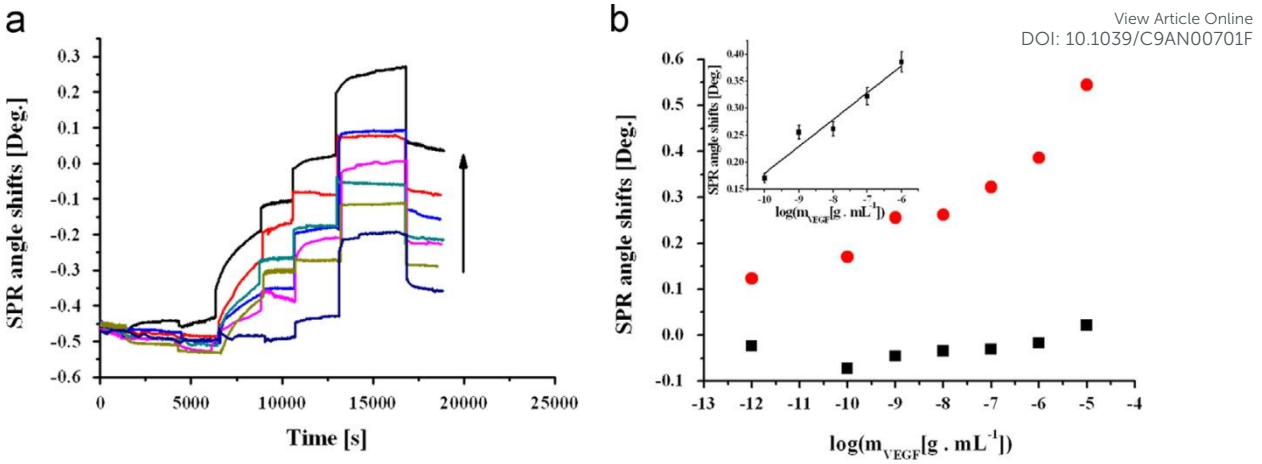

Fig 6. (a) Concentration dependence of VEGF detection from $1x10^{-12}$ to $1x10^{-5}$ g mL^{-1}, (b) the contrast of with (red points) or without (black points) the SPR signal amplification by RCA process. Reprinted with permission from (*Biosensors and Bioelectronics* 2014, 61, 83–87). Copyright (2014) Elsevier.

Another VEGF biosensor application based on DNA aptamer is presented by Cennamo *et al.*[76] The main characteristic of this system is the integration of a plastic optical fiber into the SPR platform avoiding the prism-based Kretschman configuration. Following the aptamer layer characterization, VEGF was detected directly at 81 ng mL^{-1} levels. Further experiments related to other analytical parameters such as selectivity, reusability or interference of complex matrix are not reported.

A different approach employs the immobilization of the fragment crystallizable (Fc) region of an anti-VEGF antibody, reached a linear detection range of 0.01-100 ng mL^{-1} for VEGF165 detection in human serum. The biosensor comprised of nanogold dot array that exploits the localized surface plasmon properties at narrow bandwidths. The specificity of the plasmonic biochip was tested by analyzing the interference of glucose and ascorbic acid and was also correlated with ELISA results.[77].

CEA

Another specific protein biomarker for cancer diagnosis and prognosis is the Carcinoembryonic antigen (CEA) glycoprotein. CEA is a well-established tumor biomarker with increased reported levels in several types of cancer at several locations (tumor size, staging) from the gastrointestinal tract to body organs such as liver, lung, ovary, prostate or pancreas.

Clinical determination of CEA in serum and blood plasma has been reported using SPR biosensors employing different immobilization formats. An immobilization method based on

biofunctionalized gold nanoparticles (bio-AuNPs) with either streptavidin or bovine serum albumin was described to determine CEA in blood plasma at 0.1 ng mL^{-1} levels. The assay made use of both high affinity of bio-AuNPs and lack of nonspecific binding towards the surface of the SPR sensor to improve the LOD by a factor of more than 1,000 in comparison with previous CEA determinations in undiluted plasma.[78]

CEA glycoprotein has also been detected *via* a two-channel SPR platform in spiked human serum by exploiting streptavidin affinity in different detection formats, including direct, sandwich and gold nanoparticles enhanced sandwich assays. The most sensitive detection format was obtained for the streptavidin-gold nanoparticles enhanced sandwich format allowing CEA determination at 1.0 ng mL^{-1} levels while achieving an improvement of 13.2-fold in sensitivity in comparison with the direct format. The specificity of the assay was proved against other protein cancer biomarkers, such as alpha fetal protein and prostatic specific antigen.[79]

Another recent approach[80] described the fabrication of a liquid core coupling unit as an amplification method to increase the sensitivity of a SPR biosensor by changing the liquid core refractive index. The so-called liquid core SPR coupling unit consisted of a semi-cylindrical container with an inlet and an outlet and a micro flow cell with a volume of 250 μL assembled to the SPR chip *via* a poly(dimethylsiloxane) (PDMS) layer. The applicability of the method was tested for CEA determination in real serum samples from early stage cancer patients and healthy subjects, showing an 18-fold increase of concentration in cancer samples in comparison with controls. Similarly, another novel strategy exploited[81] the surface plasmon field enhanced fluorescence (SPFS) from plasmonic nanogratings to create a protein array with a LOD of 0.36 ng mL^{-1}, showing a 10-fold signal enhancement due to the fluorescence amplification in comparison to the bare glass sensor surface.

ALCAM

Activated leukocyte cell adhesion molecule (ALCAM) is a cell surface glycoprotein of the immunoglobulin superfamily that mediates adhesion and interactions with the CD6 immune antigen. ALCAM is overexpressed in many types of cancers such as colorectal, gynecological, and pancreatic while it is associated with poor prognosis for esophageal, breast and ovarian cancers.

The analysis of ALCAM has been explored by plasmonic biosensors using both SPR imaging and LSPR detection formats. Homola's group[82] described an SPR imaging sensor that was able to detect human chorionic gonadotropin (hCG) and ALCAM with a limit of detection of 45 ng mL^{-1} in 10% diluted blood plasma. The SPRi platform comprised of a high-density protein array with 120 sensing areas. DNA directed immobilization with antibody-DNA conjugates were

microspotted on the sensor surface in combination with covalently immobilized bovine serum albumin to reduce non-specific binding.

Another approach to detect ALCAM antigen was reported by Pai *et al.*[83] using an immunoassay-based LSPR sensor. The main feature of this assay was the incorporation of polyethylene glycol adlayers in order to optimize the immobilization of gold nanorods bioconjugated to anti-ALCAM antibodies. The model was able to detect ALCAM at 1.253 ng mL^{-1} in buffer although no other analytical parameters were reported. The ALCAM gene expression has also been monitored by a LSPR design involving the use of nanoparticles as the target-specific probes capable to detect specific sequences of DNA or RNA.

4.2.2. Nucleic acids

Telomerase activity

Telomerase is a ribonucleoprotein reverse transcriptase that adds tandem telomeric repeats units $(TTAGGG)_n$ to the 3' end of telomeres in order to prevent chromosomal DNA damage. The expression of telomerase differs between normal and cancer cells. In normal cells, telomerase activity is inhibited and the telomeres length diminishes after each replication cycle. In contrast, the reactivation of telomerase is observed in over 85% of human cancer types thus inducing the division of cancer cells indefinitely by counteracting telomere shortening. Monitoring of telomerase over-expression during tumor diagnostic and therapy emerges as a promising tool while conferring to telomerase activity a valuable role as tumor biomarker.

Conventional detection methods take advantage of the formation of G-quadruplex structures by stranded repeats of TTAGGG for the development of telomere repeat amplification protocols based on PCR and electrophoresis procedures. Although extensively used, the sensitivity and reproducibility of the conventional method may be affected by the contamination of the sample and can produce false results. To overcome these limitations, several approaches have measured telomerase activity employing plasmonic biosensors.

Commonly, dual-detection mode strategies based on either fluorescence or colorimetric functionalities in combination with plasmonic properties such as SERS, Rayleigh scattering and LSPR have been described.

For instance, Wang *et al.*[84] described a LSPR biosensor combining plasmonic resonance Rayleigh scattering spectroscopy with dark-field microscopy (DFM) for *in-situ* detection and intracellular monitoring of telomerase activity in response to telomerase-based drug treatments. The biosensing method comprised core-satellites assembled nanostructures of Au50@Au13 functionalized with single chain DNA and complemented with the nicked hairpin DNA of O1. The increase of telomerase activity induced the hybridization of the telomeric repeated sequence

extended at the 3'-end of O1 to its complementary sequences at 5'-ends. Due to the elongation of O1, a rigid hairpin structure was formed and the core-satellites nanostructure of Au50@Au13 might disassemble with the release of O1. The increase of telomerase activity caused by the disassembly of Au50@Au13 was measured in HeLa cancer cell lines by the LSPR spectral shift accompanied with color changes from orange to green with a detection limit of 1.3×10^{-13} RIU.

MicroRNA

MicroRNAs (miRNAs) are short (18–24 nucleotides) non-coding RNA molecules that regulate gene expression by inhibiting the translation of mRNA. Their use as biomarkers is prominent since deregulation of miRNA signaling pathways may affect biological functions from gene expression to cellular processes, while can be also associated with cardiovascular or neurological disorders and the development of a wide number of cancer types. Due to their valuable role as protein translation regulators and the difficulties for an accurate and sensitive detection, the number of miRNAs plasmonic applications has increased remarkably in the last five years.

For instance, noninvasive monitoring of exosomes is particularly relevant in clinical analysis as they are extracellular microvesicles secreted by cells and neoplastic cell lines present in blood, urine, saliva and breast milk which contain cytosolic and plasma proteins, lipids, DNAs and RNAs. The major RNA component of exosomes is micro-RNA (miRNAs) which are of special interest for cancer monitoring as they can be associated with epigenetic changes in the recipient cells. Exosomes promote intercellular communication without direct cell-cell contact and are involved in various physiological and pathological processes such as cancer development, migration, metastasis, treatment resistance and the regulation of immune responses.

The use of exosomes has appeared to be a promising tool for the study of cancer development and metastasis. Among exosomal proteins, CD63, CD9, CD24, CD44, EpCAM, HER2, EGFR, LRP1, and LG3BP have been reported as potential biomarkers and have been already evaluated by plasmonic biosensors. For instance, two studies report the determination of exosomal expression derived from mast cell lines[85] and breast cancer cell lines[86] respectively by using a SPR commercial biosensor. Rupert *et al.* quantified the CD63 expression of the total mass of exosomes in $\mu g\ L^{-1}$ levels while the latter one was able to distinguish between the exosomal expressions of EpCAM in different types of cells in real plasma samples from healthy subjects.

Another approach involving a SPR biosensor was developed by Sina *et al.* in order to isolate bulk exosome populations and detect exosome subpopulations using the tumor-specific marker human epidermal growth factor receptor 2 (HER2). The assay was capable of identifying that 14-35% of the bulk population from a small cohort of breast cancer patients expressed HER2. Patients with

HER2+ exosomes exhibited 10-fold higher HER2 exosome concentration than HER2 and healthy patients.[87]

Alternative immobilization methods take advantage of nanoholes[87] or colloidal gold enhancement strategies to exploit nanoplasmonics.[88] For example, Park *et al.* designed a nanoplasmonic system that uses nanohole arrays as a base sensing element. Multiplexed detection of both transmembrane (EpCAM and CD63) and intravesicular (AKT1) proteins in exosome vesicles derived from ovarian cancer cells was carried out by a plasmonic sensor with 100 sensing sites, showing good correlation in the expression profiles between unperturbed cells and their exosome vesicles (see Figure 7). The detection format enabled the identification of drug-specific protein signature from drug-treated cancer cells, although the interference generated by the binding of AuNP aggregates and the use of a pair of antibodies for target capture and detection are some of its limitations.[88]

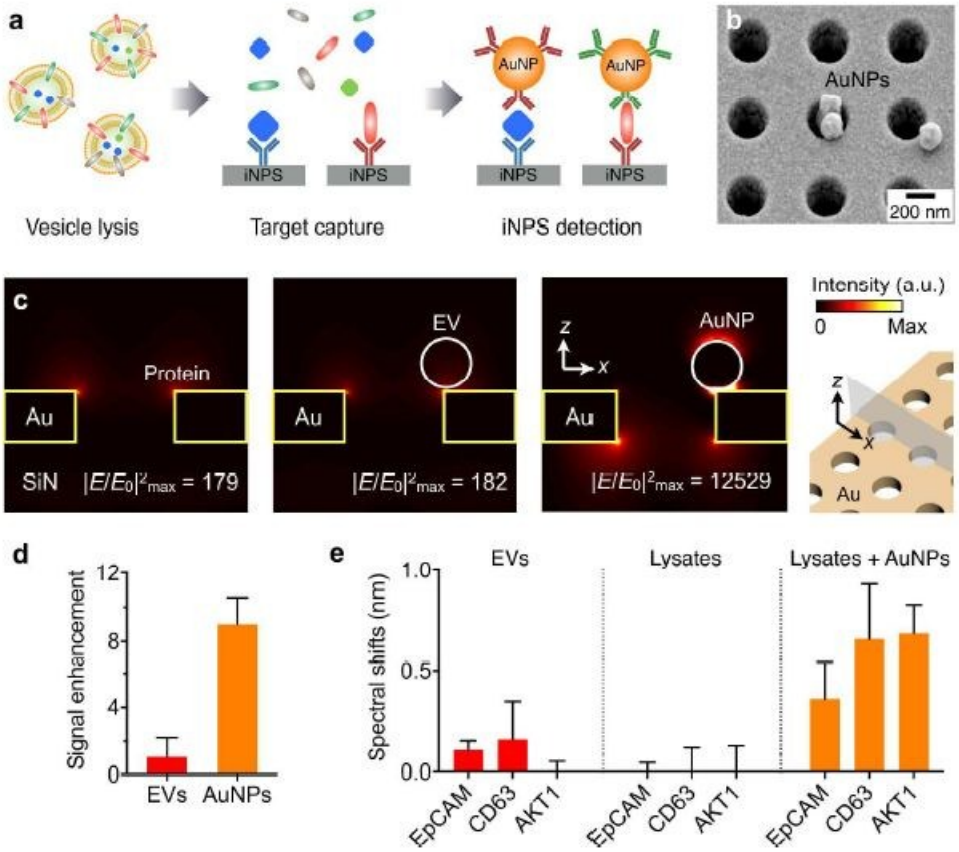

Fig.7 New intravesicular nanoplasmonic system (iNPS) assay. (a) EVs are lysed to release molecular cargos. Each target is captured on the iNPS chip *via* affinity ligands, and further labeled with Au nanoparticles (AuNPs). Note that a single assay format is used both for transmembrane and intravesicular proteins. (b) Scanning electron micrograph showing AuNPs after iNPS assay steps. (c) FDTD electromagnetic simulation. AuNP on the iNPS surface concentrates electrical fields. Compared to a protein binding (left) or a whole Extracellular Vesicles (EV) binding (middle), the field intensity enhanced up to 70-fold with AuNP (right). (d) Measured signal enhancement. Compared to EV binding, the spectral shift was about 9-fold higher when the same

concentration of AuNPs (100 nm) bound to the iNPS chip. (e) Validation of iNPS assay. AuNPs enables both membrane protein (EpCAM, CD63) and intravesicular protein (AKT1) detection with enhanced spectral shifts. The error bars represent the standard deviation of signals. Reprinted with permission from (*ACS Photonics*, 2018, 5 (2), pp 487–494). Copyright (2018) American Chemical Society.

As a last example, Di Noto *et al*.[89] exploited the colloidal properties of myeloma multiple (MM) derived exosomes by a colorimetric nanoplasmonic assay. The method allowed the determination at nanomolar concentration and cell protein binding. They demonstrate that exosomes are present in four-fold higher concentrations in myeloma multiple patients in comparison with healthy subjects, while only MM-derived exosomes have a significant binding affinity for heparin, indicating that exosomes show different binding affinities for cell-associated heparan sulfate proteoglycans.

Regarding to microRNA specific detection, LSPR and SPR biosensors have mainly exploited nanoparticle and amplification approaches. For example, Ding *et al.*[90] described the detection of real miRNA from total RNA extracted from human breast adenocarcinoma MCF-7 cells at 9 pM levels by a SPR biosensor. The detection method is based on the formation of DNA super-sandwich assemblies between target miRNA and surface bound DNA-probes after hybridization. Signal amplification was observed *via* streptavidin-biotin binding to the DNA sandwich structure. The specificity of the assay was tested against five different miRNA sequences, while the interference of complex components was evaluated by measuring spiked samples containing miRNA and total RNA, showing good recovery values (108.3%). Although the assay lacks evaluation in real biological samples, these results demonstrate its potential for discriminating a single base mismatched miRNA sequence in complex matrices.

Another laboratory custom designed SPR platform has been described for the detection of miRNA-145, a miRNA sequence involved in tumor suppression of human colon and gastric cancer cell lines. The SPR based-assay takes advantage of modified parallel tail-clamps carrying 8-amino-2′-deoxyguanosine derivatives, which are used as bioreceptors, to form stable triplex structures with their target miRNA-145. The results demonstrated that the formation of triplex structures stabilizes the hybridization and is more stable than the conventional duplex format, improving the detection limit 1.5 times (Fig. 8). This work contributes to strengthen the potential of label-free methods to profile miRNA expression by evaluating alternative approaches, such as the introduction of parallel tail-clamps bioreceptors with a short polypyrimidine track to form the most stable triplex structures.[91]

View Article Online
DOI: 10.1039/C9AN00701F

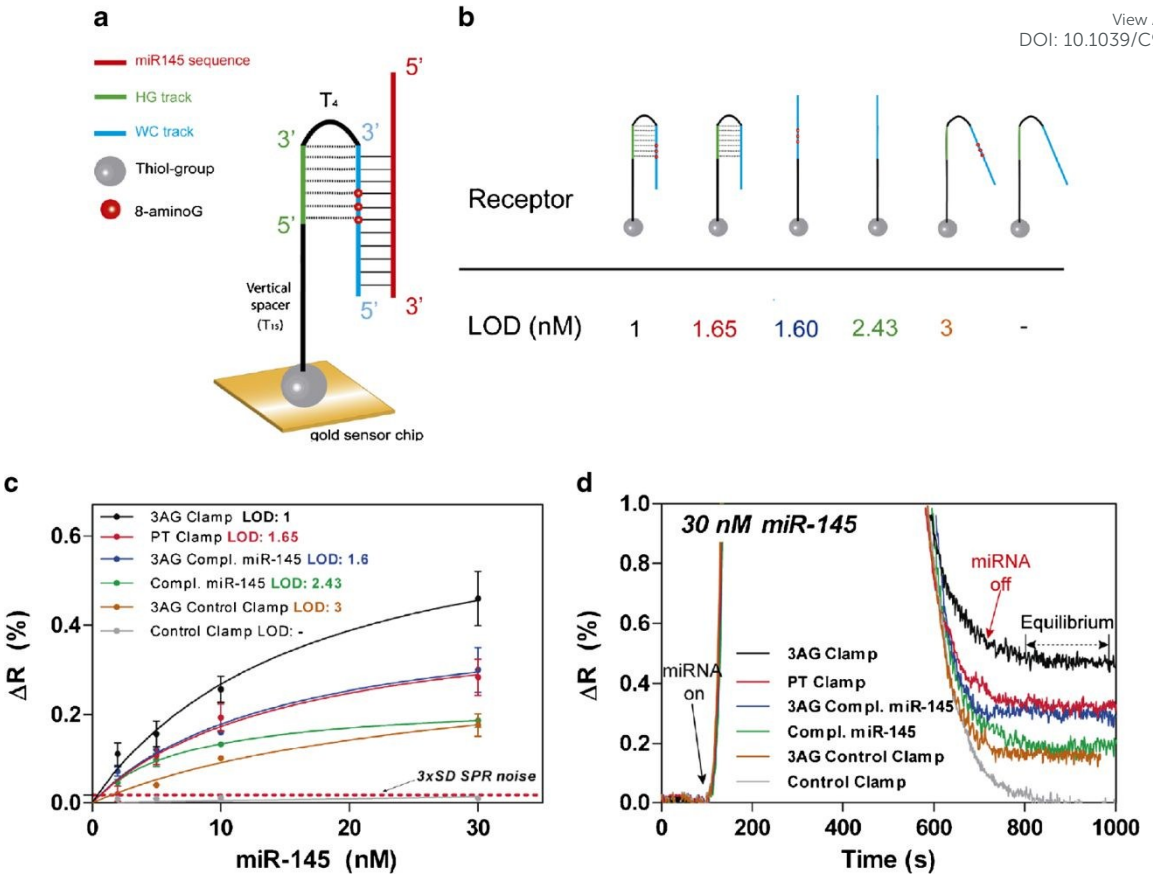

Fig. 8 Scheme of the gold sensor chip functionalized with the 3AG PT clamp bioreceptor (a). Schemes of the different bioreceptors employed for the SPR biosensor study. LODs obtained for each bioreceptor are indicated (b). SPR calibration curves of the detection of miR-145 with different bioreceptors. (c). Real-time sensorgrams of 30 nM miRNA-145 using the different bioreceptor variants. Dashed arrow indicates the equilibrium signal of the SPR sensorgrams (d)Reprinted with permission from (*Anal Bioanal Chem* 2016, 408, 885–893). Copyright (2016) Elsevier.

SPR analysis involving three-one dimensional spot arrays parallel designed for miRNA-93 capture by locked nucleic acid (LNA) immobilized probes is presented by Shmieder *et al.*[92] Two distinct amplification strategies were used to increase the assay sensitivity. First, an RNA-DNA-hybrid antibody binding to the LNA-RNA double strand after successful hybridization of miRNA-93, enabled miRNA-93 detection in RNA lysates from HEK-293 cell cultures with a limit of detection of 10 pM. Alternatively, signal amplification by using the Poly(A) polymerase enzyme after binding to the LNA probe reached a limit of detection of around 1 fM.

Several approaches involving LSPR biosensor have been reported by exploiting gold nanoparticles. Hu *et al.*[93] described trace oligonucleotide detection by measuring changes in the

dielectric constant on the surface of DNA modified gold nanoparticles after hybridization between probe single-strand DNA and miRNA at 3 nM level. The system made use of a single plasmon nanoparticle sensor based on Surface Plasmon Resonance Scattering (SPRS) to monitor a red shift during the process of hybridization due to the change of the refractive index of the surface of individual gold nanoparticles.

Similarly, a singular LSPR approach reports MicroRNA205 (miR-205) detection by monitoring the variation of the dielectric constant which causes a red shift in the LSPR scattering spectra during the hybridization of the target miRNA with a single DNA modified on the surface of a gold nanocube[94]. Measurements were carried out in serum samples with a limit of detection of 5 pM showing an improvement of three orders of magnitude in comparison with the detection efficiency of gold nanospheres (Fig.9). This achievement agrees with the theoretical analysis about the effect of the nanocrystal configuration, since the presence of more vertexes and fewer faces of polyhedral nanoparticles induce more surface plasmons in a wider energy range.

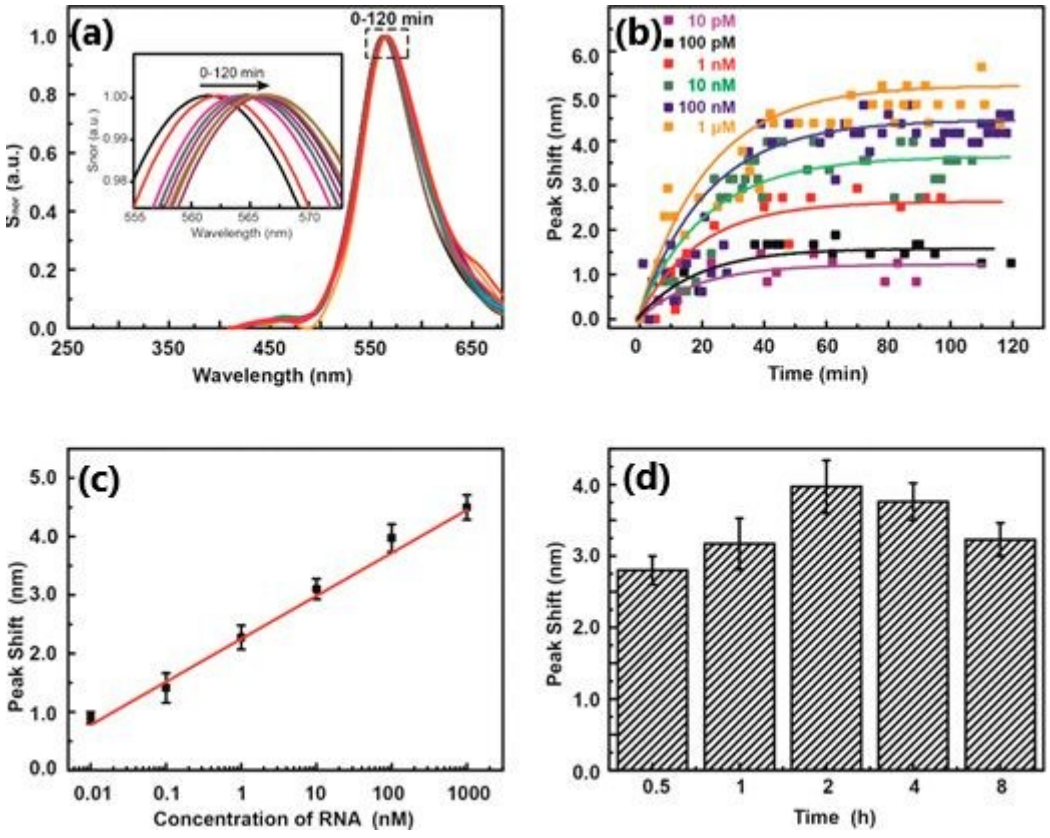

Fig 9. (a) LSPR scattering spectra of one AuNC-ssDNA probe treated with 1 μM miRNA sample at different times. (b) LSPR spectra peak redshifts with the time on various AuNC-ssDNA probes with miR-205 in different concentrations (10 pM, 100 pM, 1 nM, 10 nM, 100 nM, 1 μM). (c) Calibration curve of the LSPR peak shift versus different concentrations of miR-205 (10 pM, 100 pM, 1 nM, 10 nM, 100 nM, 1 μM). (d) LSPR Peak shift after treatment of 100 nM target miR-

205 with different modification times of 1 μM probe ssDNA. Reprinted with permission from (*ACS Sens*. 2017, 2, 1435−1440). Copyright (2017) American Chemical Society.

Sensitivities in the nanomolar range (LOD of 10 nM) were obtained for miRNa-155 detection by combining LSPR biosensing and colorimetric changes in the UV-visible spectrum[95]. The main singularity of the method consisted on the aggregation of the gold nanoparticles without ligating a linker to increase miRNA length in order to shorten the process to a single step.

Significant higher sensitivity, at attomolar levels, was achieved by Na *et al.*[96] by using a LSPR biosensor based on a 3D plasmonic nanostructure comprising gold strips on a 4-in.-scale substrate. Determination of miRNA in total RNA from extracts of cancer lines allowed for discrimination of single base mismatches (Fig. 10). Although the method has several limitations in comparison with qRT-PCR, such as labeling or gene amplification, other analytical performance parameters like response time or real-time analysis were reported to permit the integration of the 3D gold strips nanostrutrctures in point of care diagnostic devices.

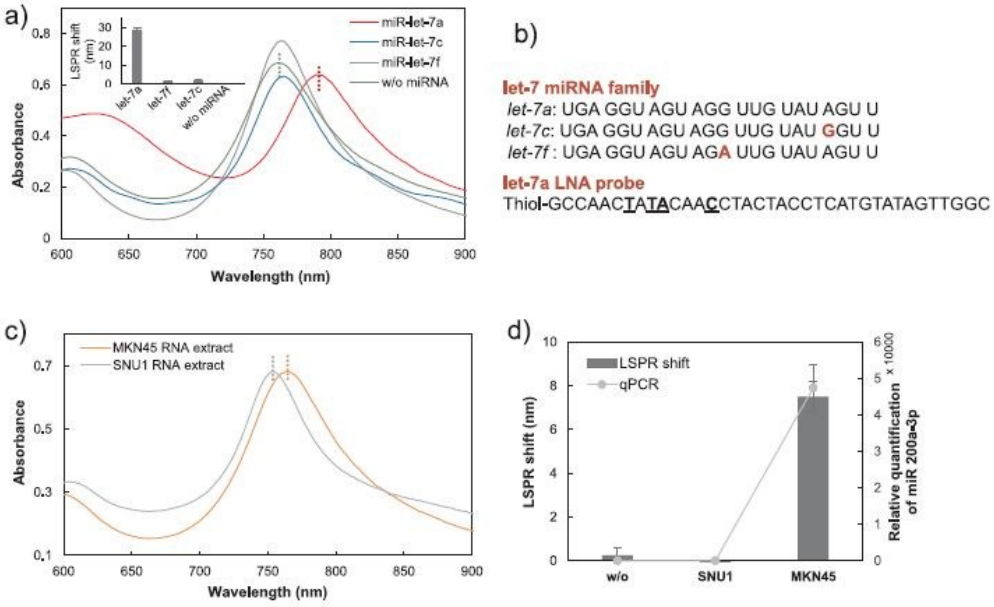

Fig. 10. Sequence specificity of the LSPR sensor for miRNA. (a) LSPR spectra of the pattern after incubation in the absence (green) or presence of miR-let-7c (blue), miR-let-7f (gray), or miR-let-7a (red, 25 nM each). (b) Probe sequence for miR-let-7a detection and sequences of miR-let-7a, miR-let-7c, and miR-let-7f. Mismatch positions in miRNA sequences are in red. LNA positions are underlined and in bold. (c) miR-200a-3p detection in total RNA extracts from human stomach adenocarcinoma cells. (d) LSPR peak shift in total RNA from human primary gastric cancer cells expressing (MKN45) and not expressing (SNU1) miR-200a-3p and quantification of miR-200a-3p in each cell line by qRT-PCR. Reprinted with permission from (*Biosensors and Bioelectronics*, 2018, 113, 39–45). Copyright (2018) Elsevier.

View Article Online
DOI: 10.1039/C9AN00701F

DNA methylation

Among the epigenetic alterations associated with the origin of cancer, DNA methylation is one of the most important mechanisms that regulate the genome imprinting while maintaining the stability to prevent mutations. DNA methylation comprises the addition of a methyl group at the fifth carbon of the cytosine ring (5-methylcytosine, 5mC) mediated by DNA methyltransferase enzymes. Since the methylation pattern is closely related to cell differentiation and normal gene expression, DNA methylation plays an important role as a promising biomarker for cancer prevention and prognosis.

In recent years, several plasmonic-based methodologies have been successfully applied to the sensitive and reliable quantification of DNA methylation. For instance, Huertas *et al.*[97] describe a SPR-based assay consisting of the monitoring of straightforward interactions between poly-purine reverse-Hoogsten hairpin probes (PPRH) and ds-DNA fragments by triple helix formation. The method proved to be effective for the specific methyl-cytosine quantification and the specific capture of ds-DNA fragments in comparison with the standard duplex-forming probes. The label-free method skips previous DNA strand de-hybridization or PCR amplification. In particular, the analysis of DNA-methylation levels of the promoter region of PAX-5 gene showed a good correlation between the sequences with a low signal variation (≤8% CV) for 35 hybridization/regeneration cycles. Additionally, no cross-reactivity results were reported by using non-specific antibody indicating its accuracy and precision for screening of other DNA modifications such as 5-hydroxymethylcytosines, 5-formylcytosine and 5-carboxylcytosine.

The analysis of methyltransferase activity plays an important role in cellular processes since it is involved not only in the status of DNA methylation but also in genome regulation and stability, thus making it a valuable biomarker with regard to cancer origin and progression.

A singular approach involving both the quantitative analysis of DNA methylation and the detection of adenine methylation (Dam) methyltransferase (MTase) activity is presented by Li e*t al*.[98] A SPR biosensor makes use of gold nanorods end-to-end assemblies, which functioned as signal-enhancing scaffolds to amplify the SPR response. The assay comprises the monitoring of the methylation process by injecting the methylation reaction solution in the first place into the fluidic channels and subsequently the end-to-end AuNR assemblies. The shift in the SPR angle after the hybridization process is enhanced by the introduction of the end-to-end AuNR assemblies showing a good correlation between the SPR angle shift and the Dam MTase concentration, with a detection limit of 0.2 U/mL (U: units of activity typically used to describe enzyme catalytic activity). The main advantage of the method comprises the capacity to screen inhibitors for Dam MTase with broad antimicrobial action, thus becoming a promising target for antimicrobial drug development.

View Article Online
DOI: 10.1039/C9AN00701F

Another SPR-based assay for DNA methyltransferase activity and the screening of its inhibitors is described by Xia *et al.*[99] The method was capable of monitoring the interaction between p53 protein and the methylation of double-stranded (ds)-DNA consensus sites consisting of a specific sequence of 5′-CCGG-3′ in which the second C base can be methylated by methyltransferase. A limit of detection of 0.09 U/mL for the methyltransferase activity was obtained due to the strong binding between the methylated ds-DNA and p53 protein. The screening of the methyltransferase inhibition demonstrated that nucleoside inhibitors are more effective than non-nucleoside inhibitors. The potential of the method for exploring DNA methylation related diseases was proved in either normal or cancer cell lysates.

4.2.3 Cells

Circulating tumor cells (CTCs) are cells within the blood stream that are released from the tumors into the blood. CTCs are scarcely present in blood since only one CTC per billion normal blood cells is circulating in patients with advanced cancer. Their presence in blood is associated with epithelial cancers and implies poor prognosis for breast, colorectal, prostate and lung cancers. Thus, characterization of CTCs by measuring either morphological properties or surface antigen expression is essential for monitoring the progression of both localized and metastatic cancer lesions. Until now, the use of plasmonic biosensors mainly rely on either the identification of cancer cell lines from the specific patterns generated by SPR signals[100] or the monitoring of cell viability through morphological changes[101]. An interesting approach is described by Hong *et al.* for the recognition of the proteolytic activity of membrane type 1 matrix metalloproteinase (MT1-MMP), a zinc proteinase extracted from invasive cancer cells. They make use of a LSPR biosensor with PEG-coated gold nanorods immobilized onto the gold sensor surface to detect the proteolytic activity of MT1-MMP. Additionally, the biosensor was capable of discriminating the proteolytic activity from whole cell lysate of two different live cancer cell lines (HT1080 and MCF7 cells). The assay sensitivity for the proteolytic activity in both MT1-MMP enzymes and cell lysates were measured by determining the maximum wavelength blue-shift changes of the LSPR spectra with regard to the response time and the MT1-MMP concentration. The kinetics proteolytic response for HT1080 cells showed higher proteolytic kinetic constant values (11.58 min^{-1}) than for MCF7 (6.10 min^{-1}) thus indicating higher proteolytic activity and overexpression of MT1-MMP proteinases.

Other interesting approach reports the monitoring of intracellular signaling events as variations of the angle of resonance of a SPR biosensor after activation of the epidermal growth factor (EGFR) from Chinese hamster ovary (CHO) cells in response to EGF induction[100]. Results showed different patterns in SPR signals when comparing carcinoma cell lines to non-tumorigenic normal cell lines. A triphasic change of the angle of resonance was observed as induction of EGF

in cancer lines whereas the activation of other receptors (as IgE, adenosine A3) produced either a monophasic change or a minimal variation of the SPR signal. These findings provide a complementary method to conventional histological techniques for the diagnosis of cancer.

Similarly, the phosphorylation of the cell surface signaling receptor VEGFR2 in intact hepatocellular carcinoma HepG2 or Huh7 cells after VEGF stimulation was reported by another SPR biosensor approach[103]. Two distinct immobilization strategies consisting of either living cells directly cultured on the sensor chip or VEGF molecules covalently attached on the sensor surface were examined. The latter strategy proved to be the most reliable method for monitoring VEGFR–VEGF interactions in terms of stability and reproducibility while distinguishable SPR sensorgrams were obtained for each cell line depending on the time required for VEGFR2 activation. The reusability of the sensor surface over more than 60 complete regeneration cycles demonstrated significant benefits over conventional analytical methods thus indicating the capacity of the sensor surface to recover the initial assay conditions without alteration of VEGF active binding sites.

Liu *et al.* reported the effect of a targeted drug (bevacizumab, anti-VEGF monoclonal antibody) on the binding between VEGFR and VEGF in live SKOV-3 carcinoma cells[104]. A customized polymer flow gasket was fabricated to attach living cells on the ceiling of the flow chamber, whereas VEGFR was immobilized on the SPR sensor chip. After stimulating the induction of VEGF from cells, bevacizumab was added to the flow chamber and the regulation effect against the VEGF-VEGFR angiogenic switch was monitored. Results showed good sensitivity and linear range for VEGF and bevacizumab interactions and the blockage of VEGF-VEGFR binding after bevacizumab addition.

4.3 Inflammation biomarkers

Inflammatory disorders comprehend a heterogeneous group of diseases that involve acute or chronic inflammation such as autoimmune diseases, allergies, hepatitis, rheumatoid arthritis, coeliac disease or transplant rejection. Monitoring of the inflammation process requires the analysis of biomarkers to allow early diagnosis and control of the illness progression while avoiding the relapse of the disease. Among inflammation biomarkers, including from cellular to molecular factors such as serum amyloid A and procalcitonin, plasmonic biosensors have mainly focused on cytokines and C reactive protein (CRP) detection.

4.3.1 Cytokines

Cytokines are soluble proteins of low molecular weight involved in cell communication as immunomodulatory agents of autocrine, paracrine and endocrine cell secretions. Additionally,

View Article Online
DOI: 10.1039/C9AN00701F

cytokines play a remarkable role in inflammatory reactions, host defense tissue damage repair, apoptosis and cancer progression. They are commonly classified as pro-inflammatory (IL-&, TNF-α) responsible of the inflammatory response and anti-inflammatory cytokines (TGF-β, and IL-4) which act as mediators of the immunological equilibrium. Monitoring the cytokine levels may provide relevant information to improve our understanding of the immune response and disease progression. Cytokines quantification primarily rely on immunoassay detection.

Multiplex cytokine analysis based on either LSPR or SPR imaging platforms appear to be the most singular approaches for cytokine detection by plasmonic biosensors. Hendriks *et al.* described an SPRi immunoassay relying on a reaction cascade which involved an antibody sandwich assay with subsequent addition of neutravidin and gold biotinylated gold nanoparticle signal enhancement[105-]. Measurements were attained for four cytokines, IL-1β, IL-6, IFN-γ, and TNF-α, in spiked synovial fluid and compared with buffer. The assay reported significantly high sensitivity (fg mL^{-1}) with an improvement of sensitivity over 40000 times and low variability when using the signal enhancement cascade. Differences in sensitivity and cross-reactivity values between cytokines were related to the affinity of the antibody pairs. The lack of validation in real human samples and signal fluctuations are limitations to be addressed in a potential POC platform. Chen *et al*[106] presented another multiplexing approach based on a LSPR biosensor microarray including eight parallel microfluidic channels fabricated by one-step microfluidic patterning and 480 nanoplasmonic sensing spots . The biosensor took advantage of antibody- conjugated gold nanorods (AuNRs) while scanning the scattering light intensity across the microarrays of AuNR conjugates with dark-field imaging optics. The assay achieved a sensitivity in the pg mL^{-1} range for six cytokines: interleukin-2 (IL-2), interleukin-4 (IL-4), interleukin- 6 (IL-6), interleukin-10 (IL-10), interferon-gamma (IFN-γ), and tumor-necrosis-factor alpha (TNF-α) in serum samples. An assay cycle was completed in 40 minutes by utilizing the entire 480 LSPR biosensor array for multianalyte detection along with ten repeated cycles including loading, incubation and washing of eight different samples. As a proof of concept, the LSPR biosensor was used to monitor the cytokine levels in serum during the immediate post-operative period of two neonates undergoing congenital heart surgery. They obtained similar results to previous studies, indicating that increased cytokine levels return to pre-operative concentrations within 48 hours of surgery. A particular strategy combining a LSPR biosensor integrated with microelectrodes pursued the enhancement of biosensing performance by applying an AC voltage to microelectrodes while scanning the scattering light intensity variation of the gold nanorods. The quantification of the IL-1β cytokine involved the functionalization of the gold nanorods followed by the monitoring of the scattering intensity change every five seconds after applying an AC bias of 180° phase difference for around 15 min[107]. The limit of detection of the assay was 158.5 fg mL^{-1} (9.1 fM) for spiked samples in PBS and 1 pg mL^{-1} (58 fM) for diluted human serum (see Figure 11).

View Article Online
DOI: 10.1039/C9AN00701F

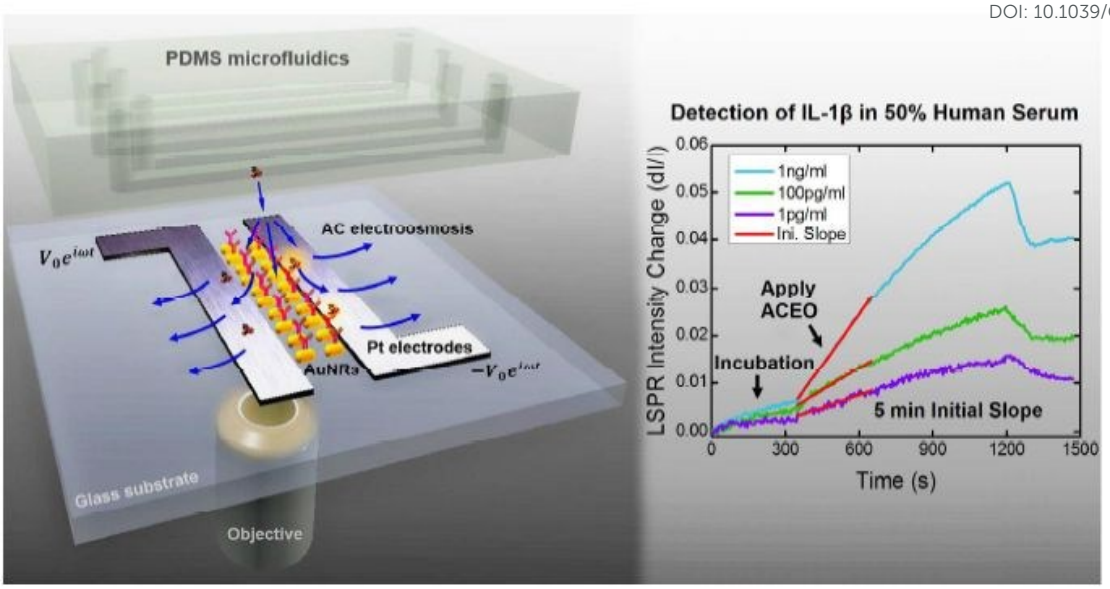

Fig. 11 Schematic and principle of AC electroosmosis-enhanced localized surface plasmon resonance (ACE-LSPR) biofunctional nanoparticle imaging. Pt microelectrodes were first patterned on a glass substrate by photolithography and metal lift-off. AuNRs were then deposited to form line-shaped sensor pattern between the microelectrodes using a microfluidic patterning technique. Reprinted with permission from (*Nano Letters*, 2017, 17, 2374-2380.). Copyright (2017) American Chemical Society.

4.3.2 CRP

C-reactive protein (CRP) is an annular blood plasma protein of liver origin with pentameric form due to five identical non-glycosylated polypeptide sub-units. CRP is associated with infectious, inflammatory conditions and other disorders. Its level increases substantially from pM to mM during an acute-phase response of inflammation. The need of continuous monitoring of CRP in clinical settings mostly rely on immunonephelometric, immunoturbidimetric and enzyme-linked immunosorbent assays (ELISA). Plasmonic biosensing of CRP has been demonstrated for over a decade. The most common approaches have focused on immunoassay applications based on either non-oriented or site-directed immobilization formats with limit of detection in the μg mL^{-1} level.

An SPR immunoassay comprised of protein A/G oriented immobilization of an anti-CRP antibody followed by direct CRP detection was described by Vashist *et al*[108]. The method achieved good sensitivity with a limit of detection of 1.2 $ngmL^{-1}$ in whole blood and serum.

Determination of CRP was also performed in EDTA plasma samples of patients showing good correlation with the clinically-accredited Roche COBAS® 8000 modular analyzer-based immunoassay and conventional sandwich ELISA-based IA (human CRP Duoset ELISA kit).

Additionally, CRP detection through aptamer-based strategies has been developed in recent years. Vance *et al.* reported an SPR imaging-oriented immobilization assay relying on the use of biotin-labeled aptamers[109]. The detection method took advantage of signal amplification by coating the aptamers with quantum dots emitting in near infrared. A limit of detection of 5 fg mL^{-1} was obtained in diluted (spiked) human serum.

Another biotinylated-aptamer SPR-based approach was employed by Wu *et al.* for CRP detection by using anti-CRP gold nanoparticles conjugates enhancement. Determination of CRP was attained by the aptamer-antibody sandwich assay in the pM or nM range for 110 times diluted human serum, while the specificity of the assay was tested against human immunoglobulin G (IgG), human serum albumin (HSA), hemoglobin (Hb), transferrin (TRF) and myoglobin (Myo)[110].

Alternatively, an immobilization method based on plasma parylene N film was used for the functionalization of the sensor biochip of a SPR biosensor. The method consisted of anti-CRP immobilization onto the parylene film with a previous introduction of peroxide, hydroxyl and carboxylic acids. Results showed that sensitivity levels needed to be enhanced since a linear detection range between 1 ng/mL and 1 g mL^{-1} was obtained.[111]

Finally, a bioactive surface consisting of a calixarene-based antibody immobilization strategy (ProLinker™ B) was evaluated by Soler *et al.* to directly detect CRP from urine and undiluted human serum samples.[112] Results were obtained for SPR and LSPR (based on nanodiscs structures) biosensors -schemes by using a laboratory nanoplasmonic biosensor device capable of working in both SPR and LSPR configurations. The comparison between both biosensing approaches showed a two-fold improvement in sensitivity for LSPR detection on gold nanodiscs (LOD(SPR) = 30.8 ng mL^{-1} and LOD(LSPR) = 16.2 ng mL^{-1}). Additional advantages of this biofunctionalization methodology on nanoplasmonic surfaces were the reduction of nonspecific adsorptions and the achievement of higher sensitivity while assuring the reproducibility and stability of the bioactive surface.

4.4 Cardiac biomarkers

Troponin forms a complex of three regulatory proteins (C, I and T) associated with muscle contraction in skeletal and cardiac muscle. Among them, troponins I and T are considered the target biomarkers for the diagnosis of acute myocardial infarction (AMI) since they are rapidly released into the bloodstream after any event associated with myocardial damage. In addition,

troponins are more sensitive and specific that other cardiac biomarkers,as creatinine (CK-MB) and or myoglobin (Mb). While the prominence of the latter ones is not supported by the number of plasmonic-based applications the presence of the former one in recent literature is increasing every year. The monitoring of increased troponin levels in blood is essential for improving the prognosis of patients while reducing deaths from heart attacks. Therefore, the rapid and real-time detection conferred by plasmonic biosensors has triggered the number of troponin applications in recent years. Most of the strategies rely on immunoassays using either SPR or LSPR biosensor platforms.

SPR detection methods commonly involve gold nanoparticles secondary signal enhancement. Pawula *et al.* describe Troponin T(tnT) detection in serum samples by using a SPR biosensor.[105] The immobilization procedure included conventional carbodiimide coupling over a thiol monolayer followed by the antibody immobilization[113]. Determination of Troponin T was attained by using either a direct or a sandwich assay with gold nanoparticles anti-tnT antibody conjugates. The optimized assay obtained a limit of detection of 0.5 ng mL^{-1} for 50 % diluted serum samples (Fig. 12). The assay could be further improved by chemical modifications to achieve enhanced sensitivity in the pM levels as required for clinical monitoring.

View Article Online
DOI: 10.1039/C9AN00701F

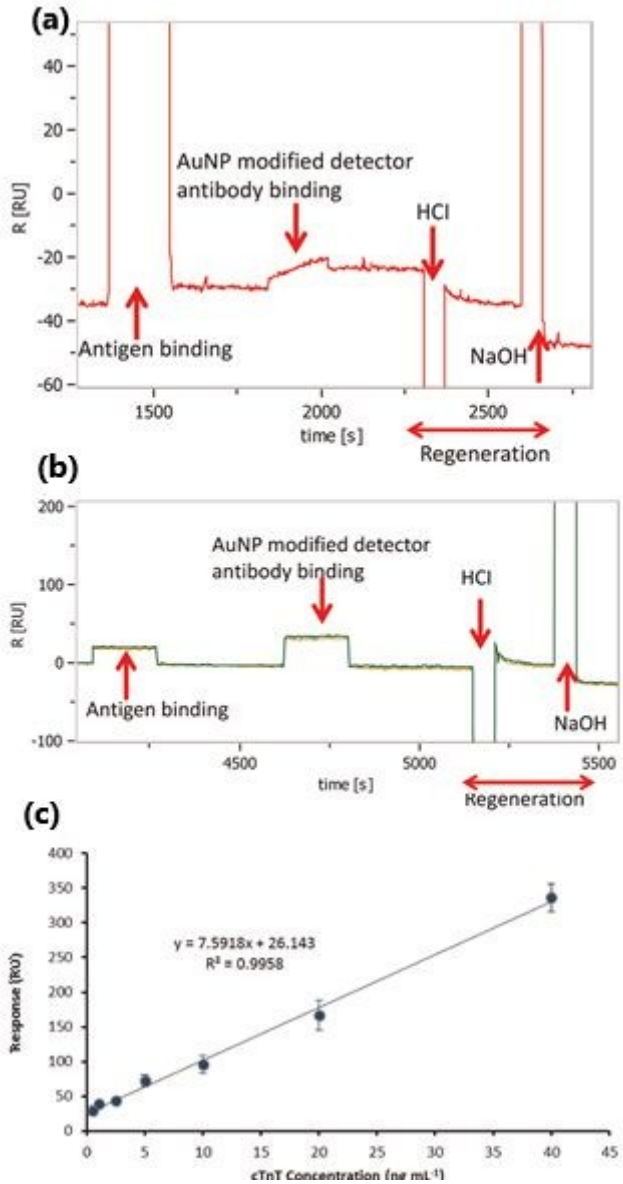

Fig. 12. Sensorgram of binding assays using AuNP modified detector antibodies on active (a) and control antibody surfaces (b). Calibration plot for the measurement of TnT in human serum using detector antibody conjugated AuNPs for amplification of the final binding response(c) (0.5 ng mL^{-1} of antigen was injected on the active sensor surface). Reprinted with permission from (*Talanta*, 2016, **146**, 823–830). Copyright (2016) Elsevier

Another SPR biosensor reported significant advancements by developing a novel troponin I detection strategy that involved both signal amplification by gold nanoparticles surface modification and the generation of a magnetic field *via* multi-walled carbon nanotubes[114]. The assay made use of a sandwich immunoassay format comprising the oriented immobilization of a capture antibody into a gold nanoparticle-polydopamine (PDA) modified sensor surface. The subsequent detection of the target analyte was carried out by conjugating the detection antibodies to nanocomposites of polydopamine and multiwalled nanotubes. The formation of the antibody

nanocomposites allowed the separation and enrichment of the target molecule while minimizing diffusion limited mass transfer and matrix interference effects. The nanocomposite assay achieved a 1000-fold improvement of the detection limit in comparison with barely PDA modified sensor surfaces. The assay was not employed for testing clinical samples.

A SPR commercial biosensor demonstrated Troponin T detection by taking advantage of PDA universal adhesive properties for immobilization of a biocompatible molecular imprinted polymer (MIP)-based receptor. The characterization of the MIP optimal properties is reported by evaluating different MIP receptors. After selecting the optimum MIP, determination of Troponin was performed in human serum at nanomolar levels[115].The improvement of sensitivity was attributed to the bottom-up functionalization approach involving the assembly of molecular nanostructures.

LSPR biosensor advances in troponin detection have allowed the determination of Troponin at attomolar level in human biological samples (plasma, serum and urine). Liyanage *et al.* described an immunoassay comprising the immobilization of the anti-TnT antibody on gold nanoprisms and the subsequent determination of troponin by measuring the LSPR wavelength shift after binding[116]. Low limit of detection at approximately 15 atM level was explained by the larger sensing surface functionalized with gold nanoprism-antibody conjugates, the appropriate SAMs length, and the number of receptor molecules that contributed to reduce the steric interference between analytes. In spite of the excellent detection limits and reproducible results reported for human body fluids, the biosensor was not capable of detecting TnT in cell extracts.

Another LSPR biosensor for TnT detection has been reported by Ashaduzzaman *et al.* by using gold nanorods (GNR) and thermosensitive poly(N-isopropylacrylamide) (PNIPAAM) to form stables anti-TnT conjugates[117]. The method attained an on/off-switching textural ability that generated a highly sensitive reversible immune interaction between 25 and 37 °C. The reversible behavior of the immunoassay was assigned to the induction of temperature structural changes by PNIPAAM that generated differential LSPR responses in the gold nanorods while monitoring the interaction between the anti-TnT and Tn-T. Following this singular approach, a limit of detection of only 8.4 fg mL^{-1} with a fast response time of only 10 seconds at 25ºC was achieved.

4.5 Singular clinical applications

Insulin

Monitoring of insulin and glycosylated hemoglobin (HbA1c) by a SPRi biosensor microarray is proposed as an innovative method for the control of diabetes instead of the successful

electrochemical glucose biosensor[118]. The dual biomarker detection format is based on the functionalization of the SPR microarray spots with insulin antibody or HbA1c-antibody (Fig. 13). To enhance the assay sensitivity, magnetic nanoparticles amine-functionalized with quantum dots and subsequently the carbodiimide-activated COOH groups were covalently attached to specific insulin and HbA1c aptamers. The conjugates formed were capable of capturing insulin and HbA1c in whole blood diluted 20-times in buffer before being magnetically separated and introduced to the SPR microarray spots immobilized with insulin antibody or HbA1c-antibody. The limit of detection using this combined SPRi fluorescence imaging assay was 4 pM for insulin and 1% for HbA1c, respectively, which are both within the clinical relevant range.

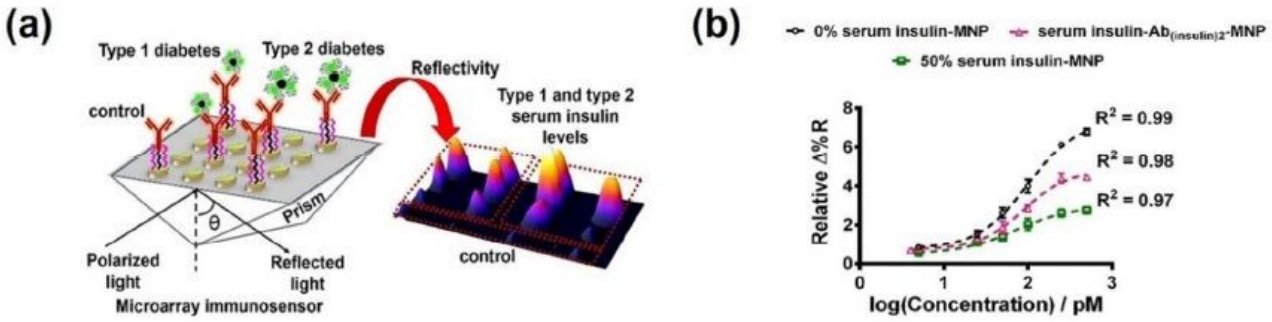

Fig. 13 (a) SPRi microarray immunosensor developed for insulin detection in human serum, and (b) SPRi responses inferring the serum matrix effect and the performance of direct vs. sandwiched 50% serum insulin immunoassay. Reprinted with permission from (*Analyst*, 2018, 143, 1544-1555.). Copyright (2018) Royal Society of Chemistry

HIV-related DNA

Human immune deficiency virus (HIV)-related DNA has been detected by SPR biosensors using entropy-driven strand displacement reactions (ESDRs) and double-layer DNA tetrahedrons (DDTs)[119]. By using the ESDRs, target DNA could be utilized by cyclic formation of a great number of double stranded DNA products, that after binding to the immobilized hairpin, could combine with DDTs nanostructures. The detection limit of HIV-related DNA was 48 fM. The major advancement over conventional methods relied on the reduction of the detection time to 6 minutes while avoiding enzyme labeling and complex chemical modifications.

Sintrom

A compact LSPR device based on gold nanodiscs has been used for the therapeutic drug monitoring of Acenocoumarol (Sintrom®), an oral anticoagulant prescribed for the treatment of a variety of thromboembolic disorders. By using a specific and reproducible label-free indirect competitive assay, acenocumarol was monitored in 1:1 plasma diluted samples[120]. The interaction

View Article Online
DOI: 10.1039/C9AN00701F

of the antibody with the custom-biofunctionalized antigen-coated surface resulted in detection levels of 0.77 nM, which are within the required clinical values for acenocumarol testing. The main contribution of the method is its potential use as complementary tool in decentralized settings as primary healthcare units.

Key analytical features and biomarker classification of the assays have been summarized in Table 1.

Table 1. Key analytical features and biomarker classification for detection in biological matrix, sensitivity and linear range

Type of biomarker	Detection format (instrument configuration, recognition element)	Matrix	Detection range/LOD	Reference
NEURODEGENERATIVE DISEASES				
Amyloid beta oligomers				
	LSPR (PEG- gold nanoparticles different sizes)	Mimicked blood	34.9 and 26 fM (Aβ 40 y Aβ42)	63
	SPR (waveguide-coupled bimetallic)	Assay buffer	22 to 440 pM (Aβ 42)	64
	SPR (fiber intrinsic coupling)	Real blood samples	0.3 pM (total and phosphorylated)	65
	SPR (multichannel platform DNA aptamers)	Undiluted plasma samples	10 fM	66
	SPR (Immmunoassay multiwalled carbon nanotubes)	Assay buffer and artificial cerebrospinal fluid	125 pM	67
Prion proteins	SPR (magnetic nanoparticles, amphiphilic copolymer)	Serum samples	0.01-1000 ng mL^{-1}	68
Amyloid fibrils (α-Synuclein proteins) Prion proteins	LSPR (gold nanorods)	Human brain samples	Plasmonic chirality down nanomolar concentrations	69
CANCER BIOMARKERS				
PROTEINS				
PSA	SPR (PSA imprinted proteins)	Spiked human samples	91 pg mL^{-1} (18 x 10^{-14}M)	70
	SPR (photolithography, microhole array fluorescence SPR interrogation)	Whole blood without treatment	142 pg mL^{-1}-1.42 μg mL^{-1}	71
	SPR (gold nanoparticles)	Serum	0.010 to 0.40 ng mL^{-1} (total PSA/ PSA free fractions)	72
	LSPR (gold nanodiscs)	Assay buffer	0.85 ng mL^{-1}	73
	LSPR (gold nanodiscs UV spectra detection)	Assay buffer Human serum	1,7 to 20.4 ng mL^{-1} LOD 1.49	74
VEGF	SPR (rolling circle amplification DNA aptamers polystyrene microsphere)	Assay buffer	$1x10^{-12}$ to $1x10^{-5}$ g mL^{-1} LOD 100 pg mL^{-1}	75
	SPR (plastic optical fiber, DNA aptamers)	Assay buffer	81 ng mL^{-1}	76
	LSPR (nanogold dot array)	Human serum	0.01-100 ng mL^{-1}	77
	SPR (gold nanoparticles)	Blood plasma	0.1 ng mL^{-1}	78

CEA	SPR (gold nanoparticles)	Spiked human serum	1.0 ng/mL^{-1}	79
	SPR (liquid core coupling)	Serum	0.5 ng mL^{-1}	80
	SPR field enhanced fluorescence (nanograting microarray)	Assay buffer PBS	0.36 ng mL^{-1} 1ng mL^{-1}	81
ALCAM	SPR imaging (DNA-directed array of antibodies)	Diluted blood plasma	45 ng mL^{-1}	82
	LSPR (gold nanorods)	Assay buffer	1.253 ng mL^{-1}	83
Telomerase activity	LSPR (Rayligh spectroscopy+dark field microscope) Gold nanostructures	Culture medium	1.3×10^{-13} IU	84
EXOSOMES	SPR	Buffer	CD 63 expression 6.3 µg mL^{-1}	85
	SPR	Plasma	Exosomal expression differentiation between cell lines	86
	SPR custom built		Identification of exosomal subpopulations 2070 exosomes/µL	87
	SPR (nanohole multiplex detection)	Culture medium PBS	Transmembrane and intravesicular proteins 10E4 exosome vesicles	88
	SPR (Colloidal gold nanoplasmonics)	Serum	Myeloma vesicles, production from patient and healthy subjects nanomolar-picomolar	89
MicroRNA	SPR (coupled with DNA super-sandwich assemblies and biotin–streptavidin based amplification.)	miRNA in total RNA samples	9 pM 1x10^{-11}M to 1x10^{-6} M	90
	SPR laboratory custom designed	human miRNAs	2 to 30 nM	91
	SPR commercial design	miRNA-93 in total RNA lysate from HEK-293 cells	10pM -1fM	92
	LSPR (gold nanoparticles + SPR scattering)	DNA probes	3 nM	93
	LSPR (red shift gold nanocubes)	DNA probes	5 pM (miRNA 205)	94
	LSPR (colorimetric UV spectrum)	DNA probes	1 nM (miRNA155)	95
	LSPR (3D nanostructure)	Total RNA Extract cell lines	13 fM: 2.6 attomole in 200 µL Single base mismatch	96
DNA methylation	SPR laboratory custom design	DNA probes	115 pM	97
	SPR (gold nanorods methyl transferase activity)	DNA probes	0.2 U mL^{-1}	98
	SPR (methyl transferase activity)	Cell lysates	3.04 nM	99
Cells	LSPR (PEG-coated nanorods)	Whole Cell lysates	Metalloproteinase proteolytic activity of cancer cell lines	102
	SPR	Culture medium assay buffer	Signalling event Change in the angle of resonance	100

	SPR	Culture medium Assay buffer	Change in the angle of resonance depending on the time required for activation.	103
	SPR (polydimethylsiloxane flow chamber gasket)	Culture medium assay buffer	VEGF binding and drug blocking-live cell lines interaction, variation of baseline	104
INFLAMMATION BIOMARKERS				
Cytokines				
IL-1β, IL-6, IFN-γ, and TNF-	SPRimaging (immunoassay)	Spiked synovial fluid	50 fg mL^{-1}	105
interleukin-2 (IL-2), interleukin-4 (IL-4), interleukin- 6 (IL-6), interleukin-10 (IL-10), interferon-gamma (IFN-γ), and tumor-necrosis-factor alpha (TNF-R)	LSPR (multiplex immunoassay arrays 480 nanoplasmonic spots antibody conjugated gold nanorods)	Serum samples	11.43 (TNF-R), 6.46 (IFN-γ), 20.56 (IL-2), 4.60 (IL-4), 11.29 (IL-6), and 10.97 (IL-10) pg mL^{-1}	106
IL-1β cytokine	LSPR (AC voltage microelectrodes)	Assay buffer Diluted human serum	158.5 fg mL^{-1} PBS; 1pg/mL human serum	107
CRP	SPR (immunoassay protein A/G oriented)	Plasma samples	1.2 ng mL^{-1}	108
	SPR imaging (oriented immobilization: biotin labelled aptamer coated NI quantum dots)	Spiked human serum	5 fg mL^{-1}	109
	LSPR (biotin labelled antibodies, anti-CRP gold nanoparticles)	Diluted human serum	10 pM-100 nM range	110
	SPR (plasma parylene film)	Assay buffer	1 $ngmL^{-1}$ and 1 gmL^{-1}	111
	SPR/LSPR (gold nanodiscs, calixarene immobilization)	Pure urine Diluted plasma	LOD(SPR) = 30.8 ng mL^{-1} LOD(LSPR) = 16.2 ng mL^{-1}	112
CARDIAC BIOMARKERS				
Troponin	SPR (immunoassay)	50% Diluted serum	0,5 ng mL^{-1}	113
	SPR (gold nanoparticles magnetic field multiwalled carbon nanotubes nanocomposite)	Spiked human serum	1.25 ng mL^{-1}	114
	SPR (molecular imprinted polymers)	Human serum	15.4 nM	115
	LSPR (gold nanoprisms antibody conjugates)	Plasma, serum and urine	15 attomolar	116
	LSPR (gold nanorods reversible immunoreaction)	Assay buffer (PbS,MES)	8.4 fg mL^{-1}	117
OTHER CLINICAL APPLICATIONS				
Insulin	SPRimaging (microarray magnetic nanoparticles, quantum dots aptamers)	Diluted whole blood	4 pM	118
HIV-related DNA	SPR (entropy-driven strand displacement reactionsand double-layer DNA tetrahedrons).	Assay buffer	48 fM	119
Sintrom	LSPR (goldnanodiscs)	1:1 diluted plasma	0.77 nM	120

View Article Online
DOI: 10.1039/C9AN00701F

Conclusions and future perspectives

Although plasmonic biosensors have exploited clinical applications for more than a decade, recent progress in nanotechnology has enabled their consolidation in a new and more advanced stage. The arrival of the new era of nanoplasmonics relies on several paramount aspects: (i) the utilization of complementary analytical performances using detection formats unable to be combined in the past (i.e. colorimetric, electrochemiluminescence, SERS or fluorescence imaging); (ii) the development of novel chemical functionalization strategies by employing top-down (lithographic, patterning, etc.) and bottom-up (nanoparticles and their self-assemblies, etc.) approaches and (iii) the selection and appropriate integration of the bioreceptors improving sensor specificity while reducing cross-reactivity and thereby eliminating false outcome. Such advancements have permitted to overcome several hurdles including poor sensitivity, limited multiplexed analysis and interference from complex biological matrices for clinical applications.

This review covers mainly analytical improvements for the determination of several types of biomarkers concerning neurodegenerative, inflammation, cancer and cardiac-related disorders by describing different plasmonics biosensor methodologies. Firstly, approaches involving modifications of conventional Surface Plasmon based-arrangements such as well-known LSPR, SPR imaging and SPR fiber optic have also contributed to achieve ultrasensitive plasmonic applications. Additionally, the use of distinct biosensor approaches with novel configuration strategies involving the combination of plasmonics with electrochemical, fluorescence or colorimetric detection has enabled the enhancement of the biosensor response while improving the assay sensitivity. The number of combined applications is represented in almost every type of biomarkers comprising from PSA and CEA cancer proteins detection to microRNA analysis.

Secondly, the design of the plasmonic sensor chip using top–down (metal nanoparticles) and bottom up (lithographic) procedures determines the stability of the biosensor device for long-term use. The fabrication of nanopatterned structures by microcontact printing, nanoimprinting and polymer or electron beam lithography provides consistent nanoarchitectures that improve the capacity of the immobilized component for interacting with the target analyte. Imprinting technology has been successfully applied to the detection of PSA, troponin or cytokine biomarkers. Similarly, the functionalization of nanomaterials by assembling nanocomposites and tagging nanoparticles for enhancing the signal response has been extensively considered in plasmonic sensing for clinical diagnosis. In particular, LSPR arrangement makes intended use of

the chemical activation of different types of nanoparticles from nanorods to nanoprisms for the detection of a broad range of biomarkers from CRP protein to living circulating tumor cells or telomerase activity.

Finally, the feasibility of any biosensor depends on the appropriate immobilization of the biorecognition element. The bioreceptors that recognize biomarkers include antibodies and aptamers to more specialized biomolecules such as cell membrane receptors, DNA probes or molecular imprinted polymers. The biocompatibility is a key aspect to consider during immobilization of the biorecognition element since the functionalization may affect its activity. The biological nature should also be preserved along measurements by generating the appropriate environment to facilitate the accessibility while maintaining the binding activity. For this reason, recent biomarker detection strategies take advantage of bottom-up surface modifications to effectively functionalize the sensor chips. The use of anti-fouling materials as PEG/OEG on nanosurfaces intends both to conserve the bioactive area from non-specific binding and to avoid the interference of complex biological media. By achieving these outcomes, the majority of plasmonic biosensors could be employed for analyzing body fluids (blood, urine or cerebrospinal fluid) with better detection limits than conventional techniques. Likewise, improved selectivity has also been demonstrated by attaining, for example, the mismatch differentiation of a single nucleic acid base pair.

In spite of the apparent progress, several aspects still need to be considered in order to reach reliable clinical applications in the future. Miniaturization, automation and integration of microfluidics are essential blocks to construct POC biosensors. Primarily, miniaturization seems an achievable goal to build efficient POC platforms owing to both the availability of lithographic techniques and the development of novel flexible materials, whilst software can be easily incorporated for the design of automatable POC devices.
Therefore, the main focus for the fabrication of POC platforms is to set the integration of microfluidics without the minimum support of additional equipment. Although several approaches are under development, particularly involving microchannels with micropneumatic or electrical pumping, more efforts are needed to develop digital microfluidic devices that enable the delivery, transport and separation of a tiny droplet of sample in a single step.

Likewise, it is worth pointing that the majority of works have concentrated on improving the analytical performance of novel and existing detection designs, whereas less attention has been paid to the integration of truly POC devices. Thus, the development of plasmonic devices has mainly focused in the improvement of sensing schemes for attaining ultrasensitive detection limits, while the incorporation of advanced software and microfluidic designs have been barely

considered. In this sense, many plasmonics works address novel functionalization strategies either to enhance the active sensing area or to prevent non-specific adhesion of proteins. This matter has been of paramount importance in order to provide antinonfouling layers that succeed in the sensor detection of biomarkers in undiluted body fluids. However, the transfer of fully-integrated devices to the clinical settings has not yet been entirely overcome and the gap between the laboratory and the market still remains.

On the other hand, validation of multiplexed detection formats, specifically for cancer, inflammation, cardiac and neurodegenerative biomarkers, is seriously needed as the first step for the clinical use of plasmonic biosensors. The second step involves both commercialization and integration of plasmonic biosensors in clinical settings for routine analysis. Since manufacturing and scale-up for mass production are the major bottleneck of clinical biosensors, extensive research on the assembly and component integration process will aid to overcome these challenges in relatively near future. Improvements in micro- and nanofabrication technologies will help to introduce plasmonic biosensors as biodiagnostic tools for the massive screening of the most prominent disorders. Furthermore, the incorporation of soft materials and wireless telemetry systems might enable wearable or implantable biosensors in the human body for non-invasive health monitoring.

Conflict of interest

There are no conflicts of interest to declare.

Acknowledgments.

ICN2 is supported by the Severo Ochoa program from Spanish MINECO (Grant No. SEV-2013-0295) and EPISENS project (TEC2012-34280).

Author information:
ORCID id:
EM: 0000-0002-6459-8107
PD: 0000-0003-2896-7611
LL: 0000-0001-5187-5358

References

1. B. Bohunicky and S. A. Mousa, *Nanotechnology, science and applications*, 2010, **4**, 1-10.
2. L. Wu and X. Qu, *Chemical Society reviews*, 2015, **44**, 2963-2997.
3. A. Qureshi, Y. Gurbuz and J. H. Niazi, *Sensors and Actuators B: Chemical*, 2012, **171-172**, 62-76.

4. S. T. Sanjay, G. Fu, M. Dou, F. Xu, R. Liu, H. Qi and X. Li, *The Analyst*, 2015, **140**, 7062-7081.
5. M. Swierczewska, G. Liu, S. Lee and X. Chen, *Chemical Society reviews*, 2012, **41**, 2641-2655.
6. O. Tokel, F. Inci and U. Demirci, *Chemical reviews*, 2014, **114**, 5728-5752.
7. J. Min, M. Nothing, B. Coble, H. Zheng, J. Park, H. Im, G. F. Weber, C. M. Castro, F. K. Swirski, R. Weissleder and H. Lee, *ACS nano*, 2018, **12**, 3378-3384.
8. P. Dey, N. Fabri-Faja, O. Calvo-Lozano, R. A. Terborg, A. Belushkin, F. Yesilkoy, A. Fabrega, J. C. Ruiz-Rodriguez, R. Ferrer, J. J. Gonzalez-Lopez, M. C. Estevez, H. Altug, V. Pruneri and L. M. Lechuga, *ACS sensors*, 2019, **4**, 52-60.
9. J. H. Guo, X. W. Huang and X. Ma, *Sensors and Actuators B-Chemical*, 2018, **275**, 446-450.
10. J. Guo and X. Ma, *Biosensors & Bioelectronics*, 2017, **94**, 415-419.
11. J. Guo, Analytical Chemistry, 2017, 89, 8609-8613.
12. C. I. L. Justino, A. C. Duarte and T. A. P. Rocha-Santos, *TrAC Trends in Analytical Chemistry*, 2016, **85**, 36-60.
13. C. I. L. Justino, T. A. Rocha-Santos, A. C. Duarte and T. A. Rocha-Santos, *TrAC Trends in Analytical Chemistry*, 2010, **29**, 1172-1183.
14. C. Chen, Q. Xie, D. Yang, H. Xiao, Y. Fu, Y. Tan and S. Yao, *RSC Advances*, 2013, **3**, 4473.
15. A. J. Bandodkar and J. Wang, *Trends in biotechnology*, 2014, **32**, 363-371.
16. S. Zhang, A. Garcia-D'Angeli, J. P. Brennan and Q. Huo, *The Analyst*, 2014, **139**, 439-445.
17. J. Sun, Y. Xianyu and X. Jiang, *Chemical Society reviews*, 2014, **43**, 6239-6253.
18. B. Špacˇková, P. Wrobel, M. Bocková and J. í. Homola, *Proceedings of the IEEE*, 2016, **104**, 2830-2408.
19. A. Abbas, M. J. Linman and Q. Cheng, *Biosensors & bioelectronics*, 2011, **26**, 1815-1824.
20. A. Zybin, V. Shpacovitch, J. Skolnik and R. Hergenröder, *Sensors and Actuators B: Chemical*, 2017, **239**, 338-342.
21. A. F. Coskun, A. E. Cetin, B. C. Galarreta, D. A. Alvarez, H. Altug and A. Ozcan, *Scientific reports*, 2014, **4**, 6789.
22. Y.-B. Shin, H. M. Kim, Y. Jung and B. H. Chung, *Sensors and Actuators B: Chemical*, 2010, **150**, 1-6.
23. J. C. Contreras-Naranjo, H. J. Wu and V. M. Ugaz, *Lab on a chip*, 2017, **17**, 3558-3577.
24. Y. T. Kim, Y. Chen, J. Y. Choi, W. J. Kim, H. M. Dae, J. Jung and T. S. Seo, *Biosensors & bioelectronics*, 2012, **33**, 88-94.
25. M. J. Linman, A. Abbas and Q. Cheng, *The Analyst*, 2010, **135**, 2759-2767.
26. Y. K. Oh, H. A. Joung, S. Kim and M. G. Kim, *Lab on a chip*, 2013, **13**, 768-772.
27. D. Zhang, L. Men and Q. Chen, *Sensors*, 2011, **11**, 5360-5382.
28. M. C. Estevez, M. Alvarez and L. M. Lechuga, *Laser & Photonics Reviews*, 2012, **6**, 463-487.
29. K. Cooper, *Micromachines*, 2017, **8**, 20.
30. H. J. Lee, A. W. Wark and R. M. Corn, *The Analyst*, 2008, **133**, 975-983.
31. M. I. Mohammed and M. P. Desmulliez, *Lab on a chip*, 2011, **11**, 569-595.
32. C. Parolo and A. Merkoci, *Chemical Society reviews*, 2013, **42**, 450-457.
33. J.-F. Masson, *ACS sensors*, 2017, **2**, 16-30.
34. C. L. Wong and M. Olivo, *Plasmonics*, 2014, **9**, 809-824.
35. M. Puiu and C. Bala, *Sensors*, 2016, **16**.
36. J. B. Fasoli and R. M. Corn, *Langmuir : the ACS journal of surfaces and colloids*, 2015, **31**, 9527-9536.
37. L. Simon, G. Lautner and R. E. Gyurcsányi, *Analytical Methods*, 2015, **7**, 6077-6082.
38. C. Liu, F. Hu, W. Yang, J. Xu and Y. Chen, *TrAC Trends in Analytical Chemistry*, 2017, **97**, 354-362.

39. Markéta Bocková, J. Slabý, T. Špringer and J. Homola, *Annual Review of Analytical Chemistry*, 2019, **12**.
40. J. A. Jackman, A. Rahim Ferhan and N. J. Cho, *Chemical Society reviews*, 2017, **46**, 3615-3660.
41. M. C. Estevez, M. A. Otte, B. Sepulveda and L. M. Lechuga, *Analytica chimica acta*, 2014, **806**, 55-73.
42. M. Svedendahl, S. Chen, A. Dmitriev and M. Ka¨ll, *Nano letters*, 2009, **9**, 4428-4433.
43. J. N. Anker, W. P. Hall, O. Lyandres, N. C. Shah, J. Zhao and R. P. V. Duyne, *Nature materials*, 2008, **7**.
44. M. Li, S. K. Cushing and N. Wu, *The Analyst*, 2015, **140**, 386-406.
45. D. K. Gramotnev and S. I. Bozhevolnyi, *Nature Photonics*, 2010, **4**, 83-91.
46. N. J. Halas, S. Lal, W. S. Chang, S. Link and P. Nordlander, *Chemical reviews*, 2011, **111**, 3913-3961.
47. H. Chen, L. Shao, Q. Li and J. Wang, *Chemical Society reviews*, 2013, **42**, 2679-2724.
48. S. Neretina, R. A. Hughes, K. D. Gilroy and M. Hajfathalian, *Accounts of chemical research*, 2016, **49**, 2243-2250.
49. K. C. Ng, F.-C. Lin, P.-W. Yang, Y.-C. Chuang, C.-K. Chang, A.-H. Yeh, C.-S. Kuo, C.-R. Kao, C.-C. Liu, U. S. Jeng, J.-S. Huang and C.-H. Kuo, *Chemistry of Materials*, 2017, **30**, 204-213.
50. J. Reguera, J. Langer, D. Jimenez de Aberasturi and L. M. Liz-Marzan, *Chemical Society reviews*, 2017, **46**, 3866-3885.
51. B. Ai, H. Möhwald, D. Wang and G. Zhang, *Advanced Materials Interfaces*, 2017, **4**, 1600271.
52. K. Chen, B. B. Rajeeva, Z. Wu, M. Rukavina, T. D. Dao, S. Ishii, M. Aono, T. Nagao and Y. Zheng, *ACS nano*, 2015, **9**, 6031–6040.
53. Y. Chen, *Microelectronic Engineering*, 2015, **135**, 57-72.
54. A. M. Lopatynskyi, V. K. Lytvyn, V. I. Nazarenko, L. J. Guo, B. D. Lucas and V. I. Chegel, *Nanoscale research letters*, 2015, **10**, 99.
55. R. Ogier, L. Shao, M. Svedendahl and M. Kall, *Advanced materials*, 2016, **28**, 4658-4664.
56. V. Peksa, P. Lebruskova, H. Sipova, J. Stepanek, J. Bok, J. Homola and M. Prochazka, *Physical chemistry chemical physics : PCCP*, 2016, **18**, 19613-19620.
57. M. C. Traub, W. Longsine and V. N. Truskett, *Annual review of chemical and biomolecular engineering*, 2016, **7**, 583-604.
58. O. Vazquez-Mena, L. Gross, S. Xie, L. G. Villanueva and J. Brugger, *Microelectronic Engineering*, 2015, **132**, 236-254.
59. S. S. Acimovic, H. Sipova, G. Emilsson, A. B. Dahlin, T. J. Antosiewicz and M. Kall, *Light, science & applications*, 2017, **6**, e17042.
60. M. Soler, M. C. Estevez, R. Villar-Vazquez, J. I. Casal and L. M. Lechuga, *Analytica chimica acta*, 2016, **930**, 31-38.
61. G. A. Lopez-Munoz, M. C. Estevez, M. Vazquez-Garcia, M. Berenguel-Alonso, J. Alonso-Chamarro, A. Homs-Corbera and L. M. Lechuga, *Journal of biophotonics*, 2018, **11**, e201800043.
62. D. Zhang, Y. Lu, J. Jiang, Q. Zhang, Y. Yao, P. Wang, B. Chen, Q. Cheng, G. L. Liu and Q. Liu, *Biosensors & bioelectronics*, 2015, **67**, 237-242.
63. H. Kim, J. U. Lee, S. Song, S. Kim and S. J. Sim, *Biosensors & Bioelectronics*, 2018, **101**, 96-102.
64. Y. K. Lee, K. S. Lee, W. M. Kim and Y. S. Sohn, *PLoS One*, 2014, **9,** e98992.
65. N. Truong Thi Vu, T. Nhu Hoa Thi, E. Nam, N. Tan Tai, W. J. Yoon, S. Cho, J. Kim, K.-A. Chang and H. Ju, *Rsc Advances*, 2018, **8**, 7855-7862.
66. S. Kim, A. W. Wark and H. J. Lee, *Analytical Chemistry*, 2016, **88**, 7793-7799.
67. S. Lisi, S. Scarano, S. Fedeli, E. Pascale, S. Cicchi, C. Ravelet, E. Peyrin and M. Minunni, *Biosensors & Bioelectronics*, 2017, **93**, 289-292.

View Article Online
DOI: 10.1039/C9AN00701F

68. Z. Lou, H. Han, D. Mao, Y. Jiang and J. Song, *Nanomaterials*, 2018, **8**.
69. J. Kumar, H. Erana, E. Lopez-Martinez, N. Claes, V. F. Martin, D. M. Solis, S. Bals, A. L. Cortajarena, J. Castilla and L. M. Liz-Marzan, *Proceedings of the National Academy of Sciences of the United States of America*, 2018, **115**, 3225-3230.
70. G. Erturk, H. Ozen, M. A. Tumer, B. Mattiasson and A. Denizli, *Sensors and Actuators B-Chemical*, 2016, **224**, 823-832.
71. J. Breault-Turcot, H.-P. Poirier-Richard, M. Couture, D. Pelechacz and J.-F. Masson, *Lab Chip*, 2015, **15**, 4433-4440.
72. Z. X. Jiang, Y. Qin, Z. Peng, S. H. Chen, S. Chen, C. Y. Deng and J. Xiang, *Biosensors & Bioelectronics*, 2014, **62**, 268-273.
73. M. Sanders, Y. B. Lin, J. J. Wei, T. Bono and R. G. Lindquist, *Biosensors & Bioelectronics*, 2014, **61**, 95-101.
74. Y. Khan, A. R. Li, L. Chang, L. D. Li and L. Guo, *Sensors and Actuators B-Chemical*, 2018, **255**, 1298-1307.
75. H. X. Chen, Y. F. Hou, F. J. Qi, J. J. Zhang, K. Koh, Z. M. Shen and G. X. Li, *Biosensors & Bioelectronics*, 2014, **61**, 83-87.
76. N. Cennamo, M. Pesavento, L. Lunelli, L. Vanzetti, C. Pederzolli, L. Zeni and L. Pasquardini, *Talanta*, 2015, **140**, 88-95.
77. H. W. Yang, R. Y. Tsai, J. P. Chen, S. P. Ju, J. F. Liao, K. C. Wei, W. L. Zou and M. Y. Hua, *ACS Appl. Mater. Interfaces*, 2016, **8**, 30845–30852.
78. T. Springer and J. Homola, *Analytical and Bioanalytical Chemistry*, 2012, **404**, 2869-2875.
79. R. Li, F. Feng, Z. Z. Chen, Y. F. Bai, F. F. Guo, F. Y. Wu and G. Zhou, *Talanta*, 2015, **140**, 143-149.
80. J. Xu and Y. Chen, *Talanta*, 2018, **184**, 468-474.
81. C. Liu, F. Meng, B. Wang, L. Zhang and X. Cui, *Analytical Methods*, 2018, **10**, 145-150.
82. M. Piliarik, L. Parova, H. Vaisocherova and J. Homola, in *Optical Sensors 2009*, eds. F. Baldini, J. Homola and R. A. Lieberman, 2009, vol. 7356.
83. J. H. Pai, C. T. Yang, H. Y. Hsu, A. B. Wedding and B. Thierry, *Analytica Chimica Acta*, 2017, **974**, 87-92.
84. K. Wang, S. Li, Y. Liu, L. Jiang, F. Zhang, Y. Wei, Y. Zhang, Z. Qi, K. Wang and S. Liu, Analytical Chemistry, 2017, 89, 7262-7268.
85. D. L. M. Rupert, G. V. Shelke, G. Emilsson, V. Claudio, S. Block, C. Lasser, A. Dahlin, J. O. Lotvall, M. Bally, V. P. Zhdanov and F. Hook, *Analytical Chemistry*, 2016, **88**, 9980-9988.
86. L. Grasso, R. Wyss, L. Weidenauer, A. Thampi, D. Demurtas, M. Prudent, N. Lion and H. Vogel, *Analytical and Bioanalytical Chemistry*, 2015, **407**, 5425-5432.
87. A. A. Ibn Sina, R. Vaidyanathan, S. Dey, L. G. Carrascosa, M. J. A. Shiddiky and M. Trau, *Scientific Reports*, 2016, **6**.
88. J. Park, H. Im, S. Hong, C. M. Castro, R. Weissleder and H. Lee, *Acs Photonics*, 2018, **5**, 487-494.
89. G. Di Noto, A. Bugatti, A. Zendrini, E. L. Mazzoldi, A. Montanelli, L. Caimi, M. Rusnati, D. Ricotta and P. Bergese, *Biosensors & Bioelectronics*, 2016, **77**, 518-524.
90. X. J. Ding, Y. R. Yan, S. Q. Li, Y. Zhang, W. Cheng, Q. Cheng and S. J. Ding, *Analytica Chimica Acta*, 2015, **874**, 59-65.
91. A. Aviñó, C. S. Huertas, L. M. Lechuga and R. Eritja, *Anal. Bioanal. Chem.*, 2016, **408**, 885–893
92. S. Schmieder, J. Weisspflog, N. Danz, M. Hubner, S. Kreth, U. Klotzbach and F. Sonntag, *Engineering in Life Sciences*, 2017, **17**, 1264-1270.
93. Y. L. Hu, L. Zhang, Y. Zhang, B. Wang, Y. W. Wang, Q. L. Fan, W. Huang and L. H. Wang, *Acs Applied Materials & Interfaces*, 2015, **7**, 2459-2466.

94. L. Zhang, J. Wang, J. Zhang, Y. Liu, L. Wu, J. Shen, Y. Zhang, Y. Hu, Q. Fan, W. Huang and L. Wang, *Acs Sensors*, 2017, **2**, 1435-1440.
95. A. Esmaeili-bandboni, S. M. Amini, R. Faridi-majidi, J. Bagheri, J. Mohammadnejad and E. Sadroddiny, *Iet Nanobiotechnology*, 2018, **12**, 453-458.
96. H.-K. Na, J.-S. Wi, H. Y. Son, J. G. Ok, Y.-M. Huh and T. G. Lee, *Biosensors & Bioelectronics*, 2018, **113**, 39-45.
97. C. S. Huertas, A. Aviñó, C. Kurachi, A. Piqué, J. Sandoval, R. Eritja, M. Esteller and L. M. Lechuga, *Biosens. Bioelectron*., *Analytical and Bioanalytical Chemistry,* 2018, **120**, 47-54.
98. X. Li, T. Song and X. Guo, *Analyst*, 2015, **140**, 6230-6233
99. Y. Xia, L. Wu, Y. Hu, Y. He, Z. Cao, X. Zhu, X. Yi and J. Wang, *Biosensors & Bioelectronics*, 2019, **126,** 269-274.
100. T. Hiragun, Y. Yanase, K. Kose, T. Kawaguchi, K. Uchida, S. Tanaka and M. Hide, *Biosensors & Bioelectronics*, 2012, **32**, 202-207.
101. A. R. Ferhan, J. A. Jackman, J. H. Park, N.-J. Cho and D.-H. Kim, *Advanced Drug Delivery Reviews*, 2018, **125**, 48-77.
102. Y. Hong, M. Ku, E. Lee, J. S. Suh, Y. M. Huh, D. S. Yoon and J. Yang, *Journal of Biomedical Optics*, 2014, **19**.
103. E. Mauriz, S. Carbajo-Pescador, R. Ordoñez, M. C. García-Fernández, J. L. Lechuga, L. M. Lechuga and J. González-Gallego, *Analyst*, 2014, **139**, 1426–1435
104. C. Liu, S. Alwarappan, H. A. Badr, R. Zhang, H. Liu, J.-J. Zhu and C.-Z. Li, *Analytical Chemistry*, 2014, **86**, 7305-7310.
105. J. Hendriks, I. Stojanovic, R. B. M. Schasfoort, D. B. F. Saris and M. Kaiperien, *Analytical Chemistry*, 2018, **90**, 6563-6571.
106. P. Y. Chen, M. T. Chung, W. McHugh, R. Nidetz, Y. W. Li, J. P. Fu, T. T. Cornell, T. P. Shanley and K. Kurabayashi, *Acs Nano*, 2015, **9**, 4173-4181.
107. Y. J. Song, P. Y. Chen, M. T. Chung, R. Nidetz, Y. Park, Z. H. Liu, W. McHugh, T. T. Cornell, J. P. Fu and K. Kurabayashi, *Nano Letters*, 2017, **17**, 2374-2380.
108. S. K. Vashist, E. M. Schneider and J. H. T. Luong, *Analyst*, 2015, **140**, 4445-4452.
109. S. A. Vance and M. G. Sandros, *Scientific Reports*, 2014, **4**.
110. B. Wu, R. Jiang, Q. Wang, J. Huang, X. Yang, K. Wang, W. Li, N. Chen and Q. Li, *Chemical Communications*, 2016, **52**, 3568-3571
111. Y.-H. Choi, H. Ko, G.-Y. Lee, S.-Y. Chang, Y. W. Chang, M.-J. Kang and J.-C. Pyun, *Sensors and Actuators B-Chemical*, 2015, **207**, 133-138.
112. M. Soler, M. C. Estevez, M. Alvarez, M. A. Otte, B. Sepulveda and L. M. Lechuga, *Sensors (Switzerland),* 2014, **14**, 2239-2258
113. M. Pawula, Z. Altintas and I. E. Tothill, *Talanta*, 2016, **146**, 823-830.
114. Q. Wu, Y. Sun, D. Zhang, S. Li, Y. Zhang, P. Ma, Y. Yu, X. Wang and D. Song, *Biosensors & Bioelectronics*, 2017, **96**, 288-293.
115. P. Palladino, M. Minunni and S. Scarano, *Biosensors & Bioelectronics*, 2018, **106**, 93-98.
116. T. Liyanage, A. Sangha and R. Sardar, *Analyst*, 2017, **142**, 2442-2450.
117. M. Ashaduzzaman, S. R. Deshpande, N. A. Murugan, Y. K. Mishra, A. P. F. Turner and A. Tiwari, *Scientific Reports*, 2017, **7**.
118. V. Singh and S. Krishnan, *Analyst*, 2018, **143**, 1544-1555.
119. W. Diao, M. Tang, S. Ding, X. Li, W. Cheng, F. Mo, X. Yan, H. Ma and Y. Yan, *Biosensors & Bioelectronics*, 2018, **100**, 228-234.
120. E. C. Peláez, M. C. Estevez, A. Portela, J. P. Salvador, M. P. Marco and L. M. Lechuga, *Biosensors & Bioelectronics*, 2018, **119,** 149-155.